Human Molecular Genetics, 2021, Vol. 30, No. 12 1111–1130

doi: 10.1093/hmg/ddab108
Advance Access Publication Date: 16 April 2021
General Article

GENERAL ARTICLE

Modeling muscle regeneration in RNA toxicity mice

Ramesh S. Yadava[1], Mahua Mandal[1], Jack M. Giese[1], Frank Rigo[2], C. Frank Bennett[2] and Mani S. Mahadevan[1,*]

[1]Department of Pathology, University of Virginia, Charlottesville, VA 22908, USA and [2]Ionis Pharmaceuticals Inc., Carlsbad, CA 90210, USA

*To whom correspondence should be addressed at: Department of Pathology, University of Virginia, MR5 Building, Rm. 3226, 415 Lane Rd., Charlottesville, VA 22908, USA. Tel: +1 4342434816; Fax: +1 4349241545; Email: mahadevan@virginia.edu

Abstract

RNA toxicity underlies the pathogenesis of disorders such as myotonic dystrophy type 1 (DM1). Muscular dystrophy is a key element of the pathology of DM1. The means by which RNA toxicity causes muscular dystrophy in DM1 is unclear. Here, we have used the DM200 mouse model of RNA toxicity due to the expression of a mutant *DMPK* 3′UTR mRNA to model the effects of RNA toxicity on muscle regeneration. Using a $BaCl_2$-induced damage model, we find that RNA toxicity leads to decreased expression of PAX7, and decreased numbers of satellite cells, the stem cells of adult skeletal muscle (also known as MuSCs). This is associated with a delay in regenerative response, a lack of muscle fiber maturation and an inability to maintain a normal number of satellite cells. Repeated muscle damage also elicited key aspects of muscular dystrophy, including fat droplet deposition and increased fibrosis, and the results represent one of the first times to model these classic markers of dystrophic changes in the skeletal muscles of a mouse model of RNA toxicity. Using a ligand-conjugated antisense (LICA) oligonucleotide ASO targeting *DMPK* sequences for the first time in a mouse model of RNA toxicity in DM1, we find that treatment with IONIS 877864, which targets the *DMPK* 3′UTR mRNA, is efficacious in correcting the defects in regenerative response and the reductions in satellite cell numbers caused by RNA toxicity. These results demonstrate the possibilities for therapeutic interventions to mitigate the muscular dystrophy associated with RNA toxicity in DM1.

Introduction

RNA toxicity is based on the concept that an expressed RNA molecule acts in a *trans* dominant manner, affecting normal cellular functions and pathways, resulting in disease. The prototype disorder for this is myotonic dystrophy type 1 (DM1), one of the most common types of muscular dystrophy. DM1 is a multisystemic disease with various manifestations including myotonia, progressive muscle wasting, cardiac conduction defects and cognitive dysfunction (1). DM1 is caused by an expanded $(CTG)_n$ repeat tract in the 3′UTR of the dystrophia myotonica protein kinase (*DMPK*) gene (2). The mutant RNA accumulates as RNA foci in the nuclei of DM1 cells (3), and through its *trans* dominant effects, adversely affects RNA-binding proteins such as muscleblind family members (MBNL1–3) and CUGBP Elav-like family member 1 (CELF1) (4). These proteins are involved in multiple aspects of RNA processing and localization (5). In addition, a number of signaling pathways and proteins including glycogen synthase kinase 3β (GSK3β), AKT, AMPK and protein kinase C (PKC) are thought to play a role in DM1 pathogenesis (6–8). In our lab, we also found that the Fn14/TWEAK signaling pathway is altered in DM1 and blocking TWEAK-Fn14 is beneficial in improving skeletal muscle pathology in a mouse model of RNA toxicity (9,10).

Muscle weakness and fatigue are the most problematic symptoms for DM1 patients (11). Progressive muscle wasting

Received: March 23, 2021. **Revised:** April 8, 2021. **Accepted:** April 9, 2021

and dystrophy are cardinal features of DM1. However, the basis for this is not well understood, and little is known about the muscle regenerative process and the effects of RNA toxicity on this. In fact, most descriptions of pathology in DM1 have commented on the surprising lack of regenerative response despite damage (12). Skeletal muscle has a remarkable capacity to repair damage due to disease or injury. This is due to a self-renewing stem-cell like population known as satellite cells [also known as muscle stem cells (MuSCs)], residing in skeletal muscle (13). In healthy adults, these cells are maintained in a unique niche on the surface of muscle fibers, in a quiescent state. They are identified by the expression of the transcription factor PAX7 (14). They account for about 1.5–2.5% of the total number of myonuclei in human adult muscle (15) and a similar percentage in adult mouse muscle (16). After damage, they proliferate and differentiate into myoblasts that go on to fuse to and repair the damaged skeletal myofibers (13). Defects in these cells and problems with muscle regeneration are seen in other muscular dystrophies and in normal aging (17–22).

Using a C2C12 mouse myoblast cell culture model, we were one of the first groups to clearly demonstrate the concept of RNA toxicity. We demonstrated the adverse effects of RNA toxicity on myogenic differentiation and the potential for its reversibility (23). Subsequent studies in this system pinpointed the defects to early aspects of myogenic differentiation and numerous key mediators of myogenesis including MyoD, p21, myogenin and miR-1 (24–27). To date, only a relatively small number of patients' satellite cells (Pax7+; MyoD−) and myoblasts (MyoD+; Pax7+/−) have been examined and primarily by cell culture. The varying disease severity and tissue samples preparation methods used have made it difficult to generalize the results (28–30). Nevertheless, there were some defects in the satellite and/or myoblast cell population, analogous to our C2C12 model. Another group reported normal myogenesis, RNA splicing defects, but increased apoptosis in DM1 primary myoblasts (31). Limited samples, lack of controls and the limitations of human tissue have made it difficult to systematically understand what defects may be present. For instance, in our search of the literature, we were unable to find studies demonstrating RNA foci in satellite cells from muscle biopsy samples collected from patients with DM1. Thus, in some recent studies, investigators have used fibroblasts from DM1 individuals to generate induced pluripotent stem cells (iPSCs), which were differentiated into myogenic cells for further studies (32–36). In one study published in 2020 (32), the authors showed that iPSC differentiated PAX7+ve cells had RNA foci, thus demonstrating the potential for PAX7+ve cells to have RNA foci. However, it is unclear if these are quiescent satellite cells (i.e. PAX7+ve/myoD−ve) as it is known that myoD is quickly activated in the majority of cultured satellite cells, within 4 h of plating (37), thus altering their character and behavior into a differentiated state (i.e. myoblast state).

Clearly, any treatment for DM1 must target and treat skeletal muscle in an effort to alleviate symptoms and disability associated with muscular dystrophy. Therapeutics development addressing this key issue is hampered without a model in which one can develop a thorough understanding of the effects of RNA toxicity on muscle regeneration, and one in which therapies could be tested to assess their effects on muscle regeneration. Satellite cells are key cellular mediators of muscle regeneration in response to damage (13). Little work has been done to explore the relevance of RNA toxicity on these primary cells involved in skeletal muscle regeneration. This knowledge gap restricts our understanding of how regeneration defects contribute to DM1 and could impact the success of developing therapies.

Here, we have now developed a mouse model of RNA toxicity (DM200) in which we study the effects of RNA toxicity on muscle regeneration and satellite cells. By shifting away from using modified cells and instead using studies of skeletal muscle, we aimed for a more *in vivo*, systematic examination of muscle regeneration/differentiation in RNA toxicity. Induced skeletal muscle damage experiments such as those using cardiotoxin or barium chloride ($BaCl_2$) have been utilized routinely to examine the regeneration process *in vivo* (38). The process of satellite cell recruitment/activation to myoblast and then myocytes has been studied extensively in these controlled damage experiments. Using this technique, the activation and timing of expression of many myogenic factors have been well characterized (13). However, the presence of the toxic RNA may alter this progression. This study is aimed at developing a model in which to characterize the effects of RNA toxicity on this process.

Results

Expression of relevant molecules associated with RNA toxicity in satellite cells

As a first step, we tried to determine if satellite cells *in situ* have RNA foci. Most, if not all, studies referencing satellite cells from patients with DM1 have involved evaluation in cell culture conditions. Satellite cells exist *in vivo* in their special niche. When they are removed from skeletal muscle, they start differentiating rapidly, become myoblasts and change expression patterns of many genes. This includes the expression of *DMPK*, which is upregulated during myogenic differentiation (39). Therefore, we screened a collection of nine muscle biopsy or autopsy samples (mostly quadriceps or biceps) from individuals with DM1 that we had obtained from collaborators or tissue banks, with the goal of studying satellite cells in their natural niche. Most of these samples were suboptimal for tissue sectioning due to freezing artifacts that resulted in poor maintenance of the histology. However, in at least three samples, we were able to obtain images of satellite cells using an anti-PAX7 antibody to label the satellite cell by immunofluorescence (IF), in combination with RNA fluorescence *in situ* hybridization (RNA-FISH) using a CY3-labeled $(CAG)_{10}$ oligonucleotide for the detection of the mutant *DMPK* mRNA. We counted 265 satellite cells between these three samples and found that on average about 26% (range of 19, 27 and 32%) of the satellite cells had evidence of RNA foci (typically one or two foci) (Fig. 1A and Supplementary Material, Fig. S1A), while the majority of satellite cells did not have detectable RNA foci. We then evaluated the expression of MBNL1 in satellite cells by combined PAX7/MBNL1 IF. MBNL1 co-localizes with RNA foci and is reported to be necessary for RNA foci formation (40). In skeletal muscle samples from two unaffected individuals, we found that MBNL1 was expressed in all the satellite cells with a roughly equal distribution between higher and lower MBNL1 staining (Supplementary Material, Fig. S1B). In the DM1 muscle samples, we were able to identify foci of MBNL1 in some satellite cells (Fig. 1B). In three DM1 muscle samples, the percentage of satellite cells with higher MBNL1 staining ranged between 1, 14 and 15%. This would be consistent with the sequestration of MBNL1 or reduction in MBNL1 signal in the nucleoplasm in DM1 cells (41,42). MBNL2 IF signal was very poor in all human samples (unaffected and DM1 muscles), and thus, we were not able to assess its expression.

For the mouse tissues, we first attempted to evaluate the expression of *Dmpk* in mouse satellite cells *in situ* using IF microscopy. Several anti-DMPK antibodies were evaluated using

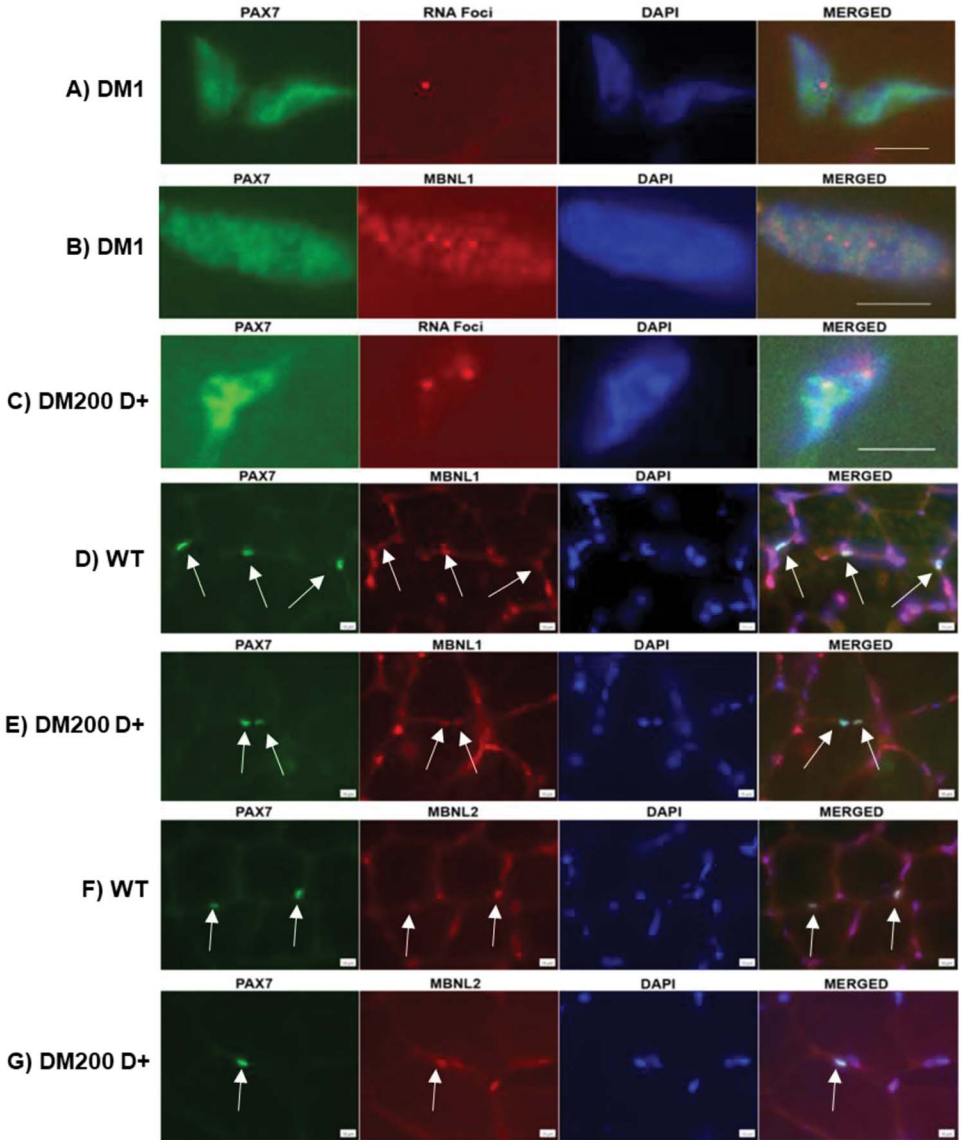

Figure 1. RNA foci and RNA binding proteins expression in satellite cells. (**A**) PAX7 IF (green) and RNA FISH (red dots) in skeletal muscle from a DM1 patient show two PAX7+ve cells, one with an RNA foci. (**B**) PAX7 IF (green) with MBNL1 IF (red) shows an example of PAX7+ve cell with MBNL1 foci. (**C**) PAX IF (green) and RNA FISH (red dots) of the TA of DM200 D+ mouse showing PAX7+ve cells with RNA foci. PAX7 IF (green) and MBNL1 IF (red) of the TA from wild-type mouse (**D**) and DM200 D+ mouse (**E**) showing PAX7+ve cells express MBNL1. PAX7 IF (green) and MBNL2 IF (red) of the TA from wild-type mouse (**F**) and DM200 D+ mouse (**G**) showing PAX7+ve cells express MBNL2. DAPI stains nuclei (blue); arrows indicate PAX7+ve cells. Scale bar = 5 μm (for A–C) and 10 μm (for D–G).

skeletal muscle tissues from *Dmpk* knockout mouse as a tissue source for validation of the antibodies. Unfortunately, none of these antibodies were adequate for accurate detection of DMPK by this method. We then did RNA-FISH/PAX7 IF in the skeletal muscles (quadriceps) of two induced DM200 mice (DM200 D+). The DM200 mouse model is a doxycycline inducible transgenic mouse model (43,44) where, upon introduction of doxycycline in the drinking water, the transgene expression is induced in the mice. We counted a total of 258 PAX7+ve cells in the tissues from the two mice and found that 11.4 and 12.7% of PAX7+ve cells had RNA foci (Fig. 1C and Supplementary Material, Fig. 1C). As in the human situation, the majority of PAX7+ve cells did not have detectable RNA foci. We also evaluated the expression of MBNL1 in PAX7+ve satellite cells using PAX7/MBNL1 IF from quadriceps muscles of wild-type (WT) mice (Fig. 1D), uninduced DM200 (DM200 D−) and induced DM200 (DM200 D+) mice (Fig. 1E) and found that MBNL1 was expressed in all satellite cells at varying levels in all groups of mice. This is similar to what we observed in the human situation. We also evaluated MBNL2 expression in satellite cells using PAX7/MBNL2 IF and found expression of MBNL2 in all satellite cells (Fig. 1F and G). Additional examples and validation of MBNL antibodies are in Supplementary Material, Figure 1.

RNA toxicity affects PAX7 expression and satellite cell number

We took advantage of the fact that the DM200 mouse model is inducible in order to study the kinetics of responses to RNA toxicity. We induced transgene expression with 0.2% doxycycline in the drinking water and collected tissues from mice at various time points over 2 weeks (0, 2, 4, 5, 7 and 14 days post induction)

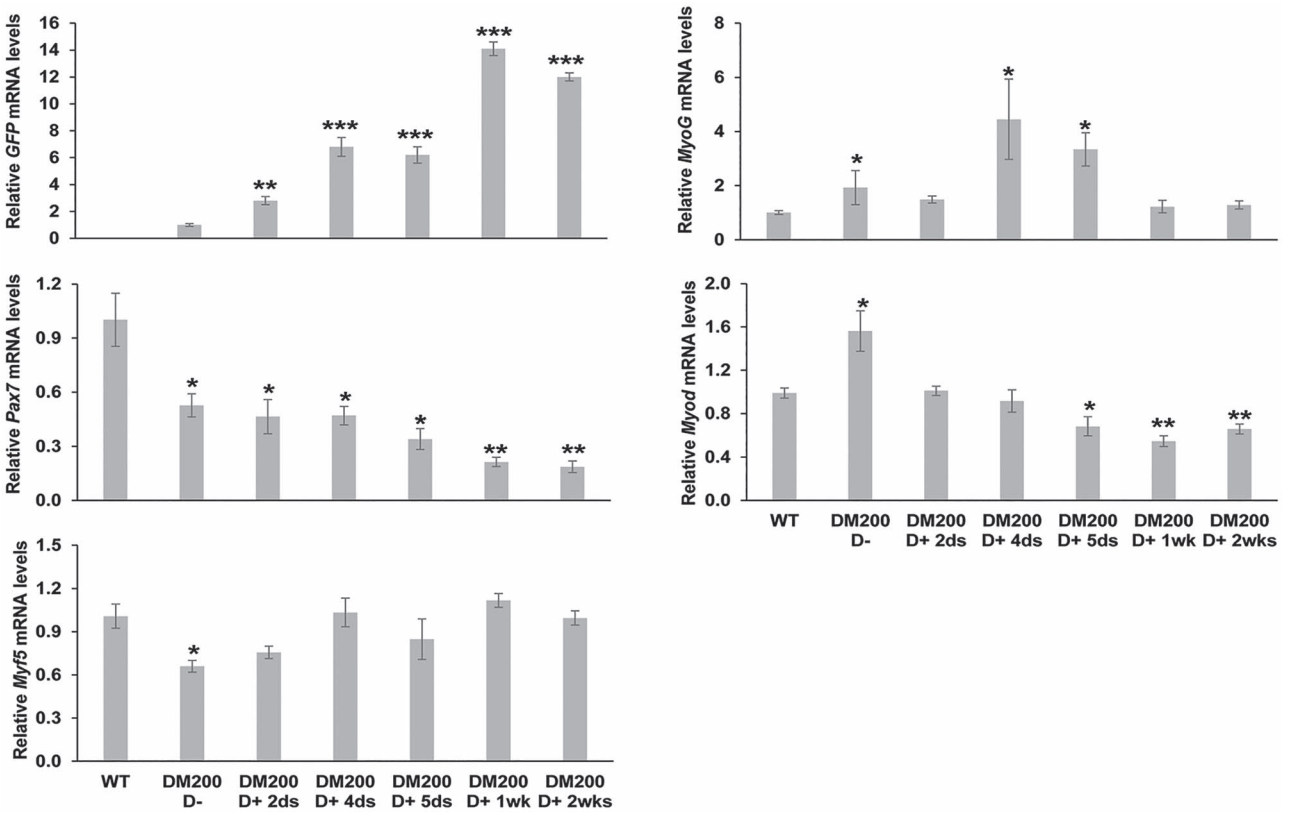

Figure 2. *Pax7* and myogenic differentiation markers are affected by expression of toxic RNA. qRT-PCR shows increased toxic RNA levels (*GFP* mRNA) in skeletal muscle (gluteus maximus) of DM200 mice induced with 0.2% doxycycline. Time course studies indicate increased *GFP* mRNA levels as early as 2 days post induction that increased over 10-fold as compared to uninduced mice (DM200 D−) by 1 week. *Pax7* mRNA levels are significantly decreased in DM200 D− tissues and decrease further with induction of toxic RNA expression (DM200 D+). qRT-PCR shows changed expression of myogenic markers (*Myf5*, *MyoG*, *Myod*) in DM200 D− mice and with toxic RNA induction (DM200 D+) during the time course (0–14 days) of the experiment. $n = 3$ mice per group; $^{*}P < 0.05$, $^{**}P < 0.01$, $^{***}P < 0.001$; Student's *t*-test; error bars are mean ± SEM.

and compared gene expression by quantitative RT-PCR (qRT-PCR) for various genes related to satellite cells (*Pax7*) and myogenic differentiation (*MyoD*, *Myog*, *Myf5*). The uninduced DM200 mice (DM200 D−) have some transgene leakiness as evidenced by a low level of GFP expression in skeletal muscle (gluteus maximus). Within 2 days, transgene induction is evident (2.8 fold, $P = 0.001$) and increased to about 6-fold by 4–5 days post induction (Fig. 2). By 7 days post induction, the GFP levels were over 10-fold increased as compared to the DM200 D− ($P = 0.0006$) and reach a steady-state level of about 10- to 15-fold induction, similar to levels previously reported for the quadriceps and gastrocnemius/soleus muscles from these mice (44,45) (Supplementary Material, Fig. S2). In the DM200 D− mice, *Pax7* mRNA levels were already reduced to about 53% ($P = 0.04$) of levels found in the gluteus maximus of wild-type mice. Upon transgene induction, *Pax7* expression steadily dropped further to about 20% of wild-type levels ($P = 0.006$) by 1 week post induction. Of the three makers of myogenic differentiation, *MyoD* showed significant changes, with levels being reduced by about 33% as compared to wild-type mice by 2 weeks post induction ($P = 0.007$), while *Myog* and *Myf5* remained relatively unchanged at 2 weeks (Fig. 2).

We then used IF microscopy to assess if the reduced *Pax7* mRNA levels were associated with any changes in the number of PAX7+ve satellite cells. Since our model system depends on doxycycline induction, we determined if doxycycline had any effect on satellite cells using wild-type mice. In tibialis anterior (TA) of wild-type mice without doxycycline induction, we found that the number of PAX7+ve cells was about 3–4 per 100 fibers (Supplementary Material, Fig. S3). This is similar to numbers reported by others (46). In the TA of wild-type mice provided with 0.2% doxycycline in their drinking water for at least 2 weeks, we found no change in the number of PAX7+ve cells or *Pax7* mRNA levels (Supplementary Material, Fig. S3). Thus, we concluded that doxycycline was not having any deleterious effect on this phenotype.

The RT-PCR data showed that DM200 D− mice already had a reduction of about 50% in *Pax7* mRNA levels as compared to wild-type mice. We thus evaluated the number of PAX7+ve cells in the DM200 D− mice as compared to wild-type mice. We found that the number of PAX7+ve cells in the quadriceps of DM200 D− mice (3.7/100 fibers) was comparable to wild-type mice (4.8/100 fibers) (Supplementary Material, Fig. 4). We also determined that the number of PAX7+ve cells in the TA muscles of DM200 D− mice (4.5 cells/100 fibers) was similar to the levels found in wild-type mice (Fig. 3). So, the reduced *Pax7* expression in the DM200 D− mice did not have any overt effect on the number of satellite cells. However, in the TA muscles of DM200 D+ mice induced for 2 weeks, we found that the number of PAX7+ve cells was reduced significantly ($P = 0.000001$) to about 1 cell/100 fibers, as compared to DM200 D− mice. This was associated with a further 50% reduction in *Pax7* mRNA levels ($P = 0.04$) (Fig. 3). Similar changes in the number of Pax7+ve cells were also seen in the quadriceps muscles of DM200 D+ mice (Supplementary Material, Fig. S4).

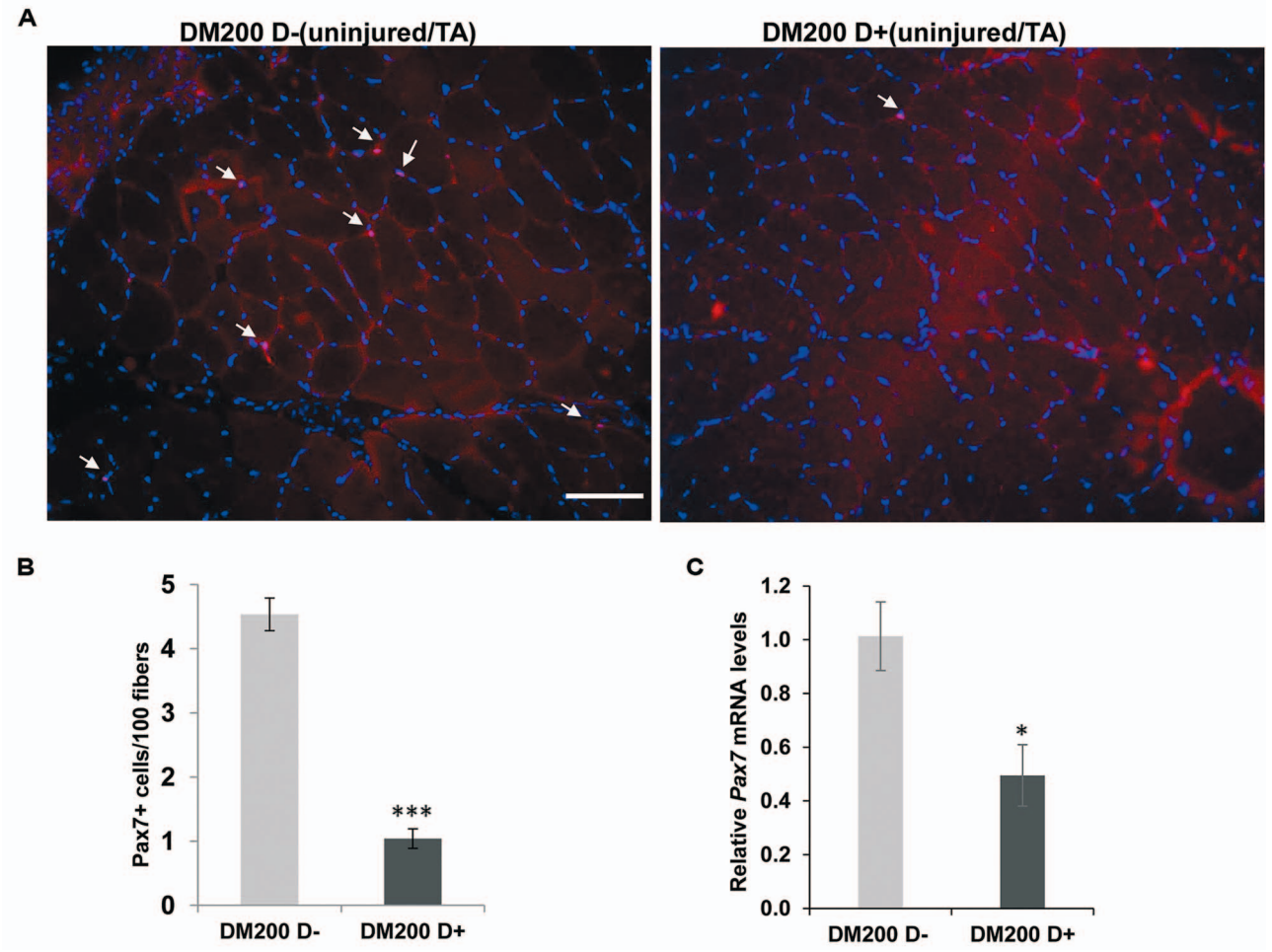

Figure 3. RNA toxicity reduced the number of satellite cells. (**A**) IF for PAX7 (red) in uninjured TA sections from DM200 D− and DM200 D+ mice. Nuclei were stained with DAPI (blue). Arrows represent PAX7+ve cells. Scale bar = 100 µm. (**B**) Quantification shows a decrease in PAX7+ cells per 100 fibers in skeletal muscle (TA) of DM200 D+ mice (2 weeks post-induction) as compared to DM200 D− mice. $n = 3$–4 mice per group; at least three non-overlapping sections/mouse; $^{***}P < 0.001$; Student's *t*-test; error bars are as mean ± SEM. (**C**) qRT-PCR shows decreased expression of *Pax7* mRNA in skeletal muscle (TA) of DM200 D+ mice (2 weeks post induction) as compared to DM200 D− mice. $n = 5$ mice per group; $^{*}P < 0.05$; Student's *t*-test; error bars are mean ± SEM.

Thus, the induction of RNA toxicity had a deleterious effect on the number of PAX7+ve satellite cells in multiple muscles.

RNA toxicity affects muscle regeneration

In order to study the effects of RNA toxicity on muscle regeneration, we decided to use an induced damage protocol that is a standard for studying muscle regeneration in mice. This typically uses the TA muscle and utilizes some form of induced damage such as the injection of cardiotoxin, barium chloride ($BaCl_2$) or freeze-induced damage (38). These agents cause focal myonecrosis, which is then healed by muscle regeneration over a period of 4 weeks. Such approaches have been used for decades and the response to damage and subsequent repair and the associated histologic and molecular changes as well as cellular responses have been well characterized and standardized (13,16,47–49). We evaluated a cohort of male and female DM200 mice, 2 months old, by electromyography (EMG) and electrocardiography prior to doxycycline induction. All mice had no myotonia and normal electrocardiogram (ECG). Then, we induced the transgene with 0.2% doxycycline in the drinking water in half the cohort (DM200 D+), with the other half remaining as an uninduced control group (i.e. DM200 D−). After 2 weeks, we performed EMGs and ECGs and confirmed that the induced mice had relevant DM1 phenotypes as previously described (44). At that point, we injected 100 µl of a 1.2% $BaCl_2$ solution into the right TA and an equivalent volume of PBS into the left TA as an undamaged control, in both groups. We collected tissues from subsets of mice from the DM200 D− and the DM200 D+ groups at various time points corresponding to the presence of satellite cell, myoblasts, myocytes and myofibers (0, 5, 14, 28 and 56 days). The schema for this protocol is represented in Figure 4A.

The $BaCl_2$ causes myonecrosis rapidly. In healthy muscle that is damaged this way, there is subsequently an inflammatory response involving neutrophils and macrophages over the next 3–4 days at which point there is an exuberant increase in the number and activation of satellite cells by day 5. This activation is accompanied by the upregulation of MyoD, which marks a commitment of the satellite cells to a differentiated state. The satellite cells differentiate to myoblasts (MyoD+ve), which then differentiate (marked by increased myogenin), and then fuse leading to the appearance of newly regenerating immature myofibers [marked by the expression of embryonic myosin heavy chain (MYH3)].

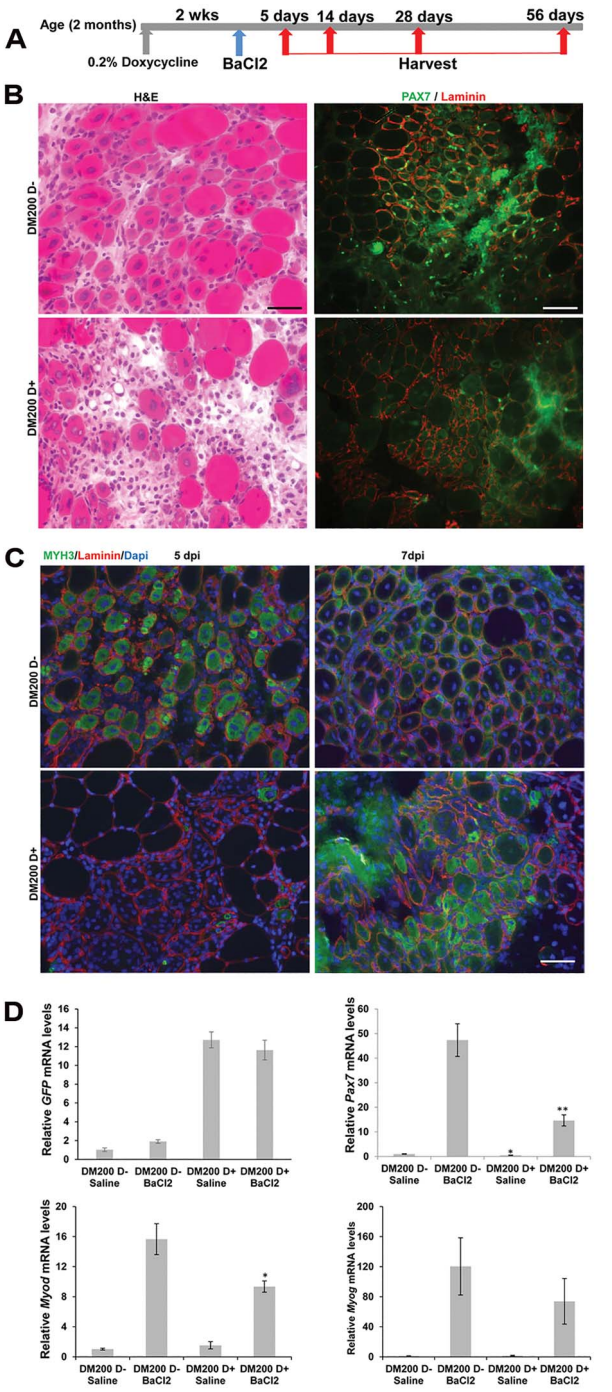

Figure 4. Skeletal muscle regeneration is delayed early by RNA toxicity. (**A**) Schematic showing the experimental design for single injury used in this study. (**B**) Representative images of H&E staining and PAX7 IF (green) at 5 days after injury by $BaCl_2$ in DM200 D− and DM200 D+ TA muscles. The H&E shows persistence of inflammatory response and lower number of regenerating fibers in DM200 D+ mice, and the PAX7 IF shows a deficit in satellite cell numbers in response to damage. (**C**) MYH3 IF(green) of TA muscles at 5 (left) and 7 (right) days post injury (dpi) demonstrates reduced and delayed expression of this marker of regeneration in DM200 D+ mice as compared to DM200 D− mice; laminin (red), nuclei are stained with DAPI (blue). (**D**) qRT-PCR shows that expression of *GFP* mRNA is induced to similar levels in control and $BaCl_2$ injected legs of DM200 D+ mice. At 5 days post $BaCl_2$, the levels of *Pax7* and *MyoD* induction in response to damage are reduced significantly in the TA muscles of DM200 D+ mice as compared to DM200 D− mice. Saline represents the contralateral leg in each mouse, injected with PBS. $n = 5$ mice per group; $^{*}P < 0.05$, $^{**}P < 0.01$; Student's *t*-test; error bars are mean ± SEM. Scale bars = 50 μm.

We examined the histology of the TA muscles collected at 5 days post damage. We focused on areas where the damage was evident (i.e. myonecrosis and inflammation). In the DM200 D− mice, hematoxylin and eosin (H&E) staining consistently showed evidence of regeneration with the presence of many small regenerating fibers with central nuclei (a marker of myofiber regeneration after damage) (Fig. 4B). In marked contrast, the DM200 D+ mice showed far fewer regenerating fibers and more persistence of the inflammatory cellular response (Fig. 4B). PAX7 IF on these tissues revealed a dramatic and robust increase in the number of PAX7+ve cells in response to damage in the DM200 D− TA muscles (Fig. 4B). Whereas, the response in DM200 D+ TA muscles showed far fewer PAX7+ve cells (Fig. 4B). The average number of PAX7+ve cells per 20× field was 29 ± 5 in the DM200 D− mice, as compared to only 4 ± 1.4 in the DM200 D+ mice ($P = 0.00006$). IF microscopy was used to determine the expression of embryonic myosin heavy chain (MYH3), a marker of nascent myofiber formation. In the TA muscles from the DM200 D− mice, we observed that the majority of the small fibers with central nuclei expressed MYH3 (Fig. 4C). In contrast, in the DM200 D+ mice, far fewer centrally nucleated myofibers expressed MYH3 (Fig. 4C), suggesting a delay in muscle regeneration. This was confirmed by assessing the expression of MYH3 in tissues collected 7 days post damage, where we saw that in the DM200 D+ mice, more myofibers were now expressing MYH3, whereas in the DM200 D− mice it was diminishing, as the myofibers in these mice were transitioning to a more mature structure and organization (Fig. 4C).

Quantitative RT-PCR was done on RNA extracts from TA muscles collected 5 days after damage (Fig. 4D). The GFP transgene was induced in the DM200 D+ TA muscles to about 12 times the levels found in the TA muscles of DM200 D− mice, similar to what was mentioned earlier. The $BaCl_2$ damage did not change the level of transgene induction (compare DM200 D+ saline to DM200D+ $BaCl_2$). In response to the $BaCl_2$-induced damage, the *Pax7* mRNA levels in the DM200 D− mice rose to about 50 times that in undamaged muscle (i.e. DM200 D− $BaCl_2$ versus DM200 D− saline). In contrast, in the DM200 D+ damaged muscle (DM200 D+ $BaCl_2$), the *Pax7* mRNA levels were only about one-third of that in the DM200 D− $BaCl_2$ damaged muscle ($P = 0.001$). The *MyoD* mRNA levels in DM200 D− damaged muscle rose to about 16 times that in undamaged muscle. However, in the DM200 D+ muscle, it was only 9-fold ($P = 0.04$). Similarly, the myogenin levels in the damaged DM200 D+ muscles were only 60% of those in damaged DM200 D− TA muscles; however, this did not reach statistical significance.

The preceding analyses are all consistent with a delay in muscle regeneration and a deleterious effect on satellite cell numbers as early as 5 days post damage. We evaluated if this delay persisted by assessing muscle regeneration through H&E histologic analysis and muscle fiber size determination. For each time point, we analyzed tissues from three to five different mice for each group and at least three sections per mouse. In order to determine the effects of RNA toxicity in the absence of any damage, from each mouse, we used the TA muscles that had been injected with saline (PBS). Fiber size analyses on H&E sections from tissues collected at 5, 14 and 28 days post saline injection showed no significant differences between DM200 D− and DM200 D+ TA muscles (Supplementary Material, Fig. S5). In contrast, at 5 days post $BaCl_2$ damage, as mentioned previously (Fig. 4B), there was a clear difference in the number of fibers with central nuclei (indicating regenerating fibers), with increased numbers in the DM200 D− group, and a persistence of inflammatory cells in the DM200 D+ muscles (Fig. 5). We summed the

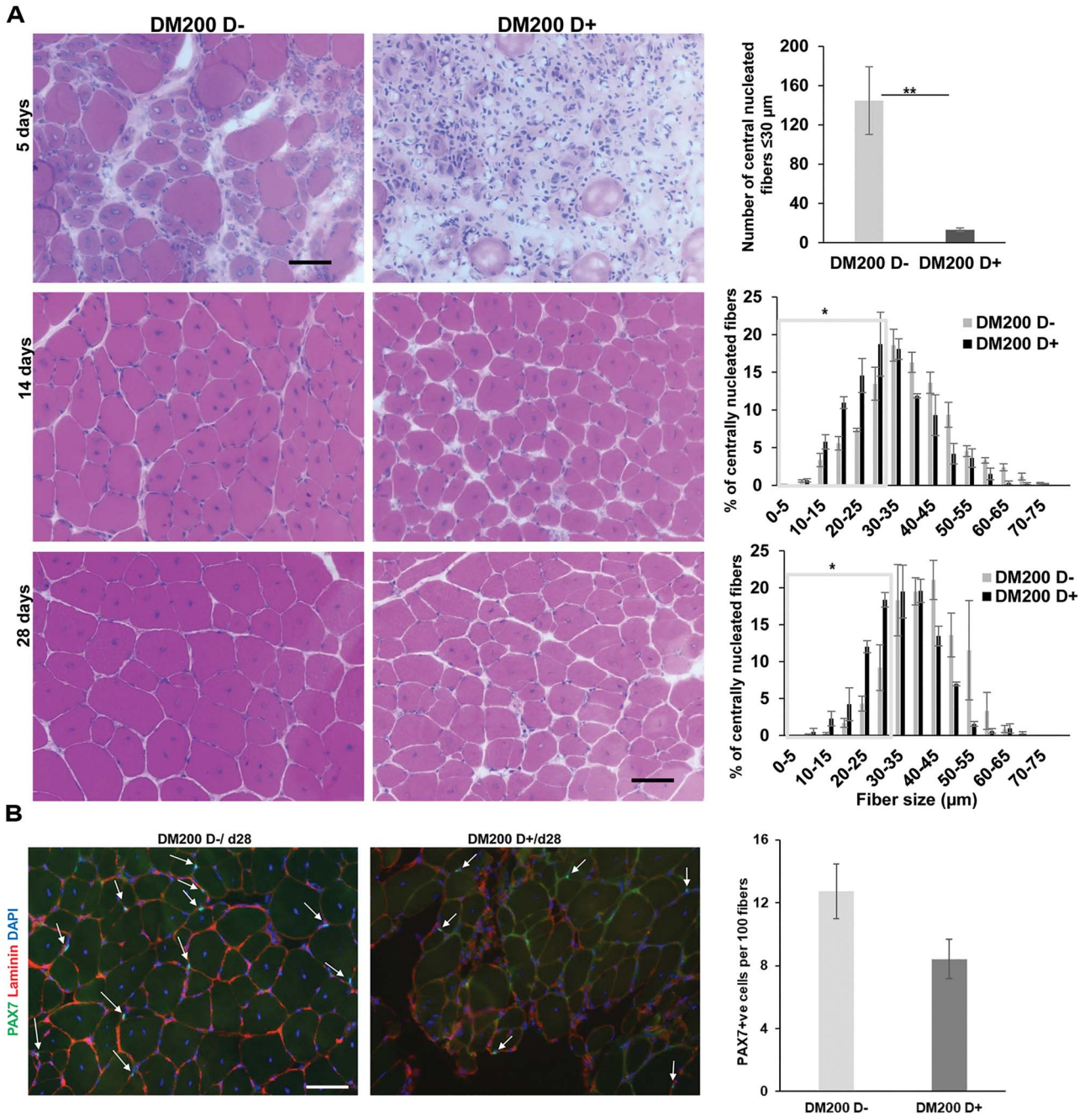

Figure 5. Muscle histology and fiber sizing confirm persistent delay in muscle regeneration and reduced satellite cell numbers in RNA toxicity mice. (**A**) Representative H&E staining of TA muscle sections 5, 14 and 28 days post injury (dpi) in the DM200 D− and DM200 D+ mice; scale bars = 50 µm. Graphs on right—the top graph represents quantification of the number of centrally nucleated fibers <30 µm (i.e. regenerating fibers) at 5 days post damage. The bottom two graphs at 14 and 28 days post damage represent a fiber size distribution plot with fibers <30 µm in the boxed area; $n = 3$–5 mice per group; five non-overlapping sections/mouse; $^{*}P < 0.05$; Student's *t*-test; error bars are mean ± SEM. (**B**) PAX7 IF (green) showing PAX7+ve cells (arrows) in DM200 D− and DM200 D+ TA muscles 28 days post injury; laminin (red); nuclei (blue); scale bars = 50 µm. Quantification shows a reduced (but not statistically significant) number of PAX7+ve cells in DM200 D+ mice; $n = 3$ mice/group; 5–6 non-overlapping sections counted/mouse; error bars are mean ± SEM.

data from four mice per group and found that the damaged DM200 D− muscles had a total of 607 fibers with central nuclei, whereas the damaged DM200 D+ muscles had only 58 such fibers. Of these, we counted the number of fibers with central nuclei that were less than 30 microns, as a better indicator of nascent regenerating fibers. In the DM200 D− mice, we found about 145 fibers/mouse (total 579 of 607 fibers) that met this criteria, whereas in the DM200 D+ mice, there were only about 13 fibers/mouse (53 of 58 fibers) ($P = 0.009$) (Fig. 5A). We then sought to determine if differences persisted beyond this time point. Typically, healthy skeletal muscle, by 14 days post damage, is healing and remodeling with increasing maturation of regenerated fibers. Histologic analyses typically show that the majority of regenerating fibers exhibit central nuclei and the muscle architecture more closely resembles healthy muscle. Therefore, using H&E histology and subsequent fiber sizing, we analyzed the fiber size diameter of central nucleated fibers at 14 days post damage in the DM200 D− and the DM200 D+ mice. The

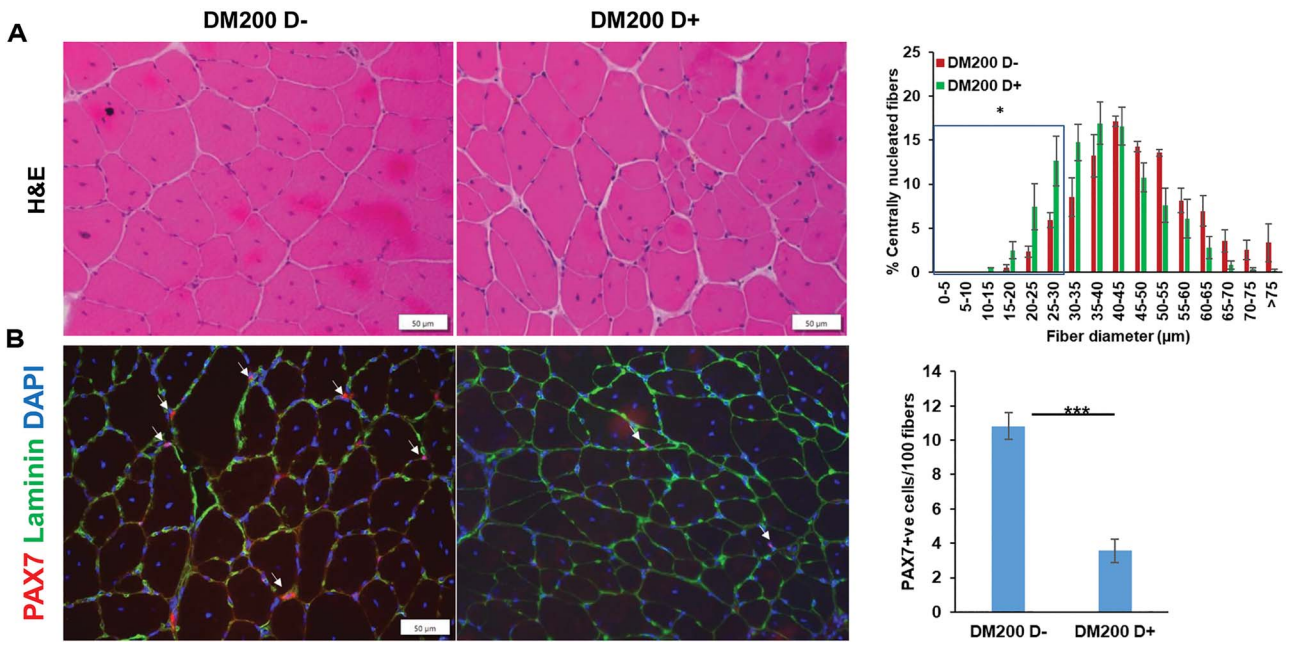

Figure 6. Delayed regeneration persists to 56 days post damage. **(A)** Representative H&E staining of TA muscle sections 56 days post injury in the DM200 D− and DM200 D+ mice, showing more fiber size variability in the DM200 D+ mice; scale bars = 50 μm. Graph on right represents a fiber size distribution plot with fibers <30 μm in the boxed area; $n = 3$–5 mice per group; five non-overlapping sections/mouse; $^{*}P < 0.05$; Student's *t*-test; error bars are mean ± SEM. **(B)** PAX7 IF (red) showing PAX7+ve cells (arrows) in DM200 D− and DM200 D+ TA muscles 56 days post injury; laminin (green); nuclei (blue); scale bars = 50 μm. Quantification shows a significantly reduced number of PAX7+ve cells in DM200 D+ mice; $n = 3$ mice/group; 5–6 non-overlapping sections counted/mouse; $^{***}P < 0.001$; Student's *t*-test; error bars are mean ± SEM.

tissue sections showed that the DM200 D− mice seemed to have more intact architecture with larger fibers. Fiber size analyses confirmed this and showed that the DM200 D+ mice had a statistically significant increased percentage of smaller regenerated fibers (<30 μm) ($P = 0.016$) as compared to the DM200 D− mice (Fig. 5A). This difference in fiber size distribution persisted at 28 days post damage with the DM200 D+ mice showing a higher percentage of smaller regenerated fibers ($P = 0.013$) (Fig. 5A). The number of PAX7+ve cells in the DM200 D+ TA muscles (8 ± 2/100 fibers) was trending lower than in the DM200 D− TA muscles (13 ± 3/100 fibers) at this time point ($P = 0.11$) (Fig. 5B).

To determine if the delayed histology and the reduced satellite cell number at 28 days post damage would catch up with time, we evaluated damaged TA muscle 56 days after $BaCl_2$ administration. At this time point, the DM200 D+ mice still showed evidence for delayed regeneration with an increased proportion of smaller central nucleated fibers (<30 μm) ($P = 0.05$) as compared to DM200 D− mice (Fig. 6A). In addition, the number of PAX7+ve cells was now significantly lower in the DM200 D+ mice (3.6 ± 1.2/100 fibers) as compared to DM200 D− mice (10.8 ± 1.6/100 fibers) ($P = 0.008$) (Fig. 6B). This suggested that the RNA toxicity impaired the ability to maintain a pool of satellite cells in damaged muscle. We also compared the DM200 D− mice to WT D+ mice and found no difference in fiber size distribution or PAX7 numbers, 56 days post damage (Supplementary Material, Fig. S6). This suggested that the response to damage between DM200 D− mice and wild-type mice was alike.

Repeated damage brings out a dystrophic phenotype in RNA toxicity mice

Muscular dystrophy is thought to progress from repeated damage and depletion of the regenerative response. This leads to replacement of healthy muscle tissue by fibrous and fatty tissue, which is the hallmark of the dystrophic phenotype. One way to model this in mice is to use repeated episodes of induced damage. In a healthy mouse, proper repair is essentially achieved by 28 days post damage, and the mouse is able to respond in a similar way to a repeated damage event. However, in a compromised mouse, repeated damage may bring out a dystrophic phenotype, especially in mice in which the satellite cells are compromised in number or function (50). Given the delay in regeneration and depletion of satellite cells caused by RNA toxicity, we sought to determine if this would affect the ability of the DM200 mouse to respond to repeated episodes of damage. Therefore, we designed an experiment where we damaged the TA of wild-type and DM200 D+ mice with $BaCl_2$, waited 28 days and then repeated the damage with a second administration of $BaCl_2$. This was followed by tissue collections at 5 and 14 days after the second damage event for histologic evaluations (Fig. 7A).

The most striking difference in the H&E histologic analyses between the WT D+ mice and the DM200 D+ mice at 5 days post re-damage was the obvious and increased number of fat droplets in the damaged TA muscles of DM200 D+ mice as compared to the more orderly repair in the WT D+ tissues (Fig. 7B and Supplementary Material, Fig. S7A). The presence of oil droplets was confirmed with Oil Red O staining, which stains for fat droplets (Fig. 7B and Supplementary Material, Fig. S7B). Further confirmation was obtained by IF using an anti-perilipin 1 (PLIN1) antibody, which showed marked increase in the presence of PLIN1 in the DM200D+ TA muscles (Fig. 7C). Perilipin is a protein that associates with the surface of lipid droplets (51). The presence of large amounts of fat droplets is abnormal and is consistent with impaired repair and phenotypes seen with muscular dystrophy.

As mentioned, the H&E staining of WT D+ TA muscles at 5 days post re-damage showed a more organized histology of

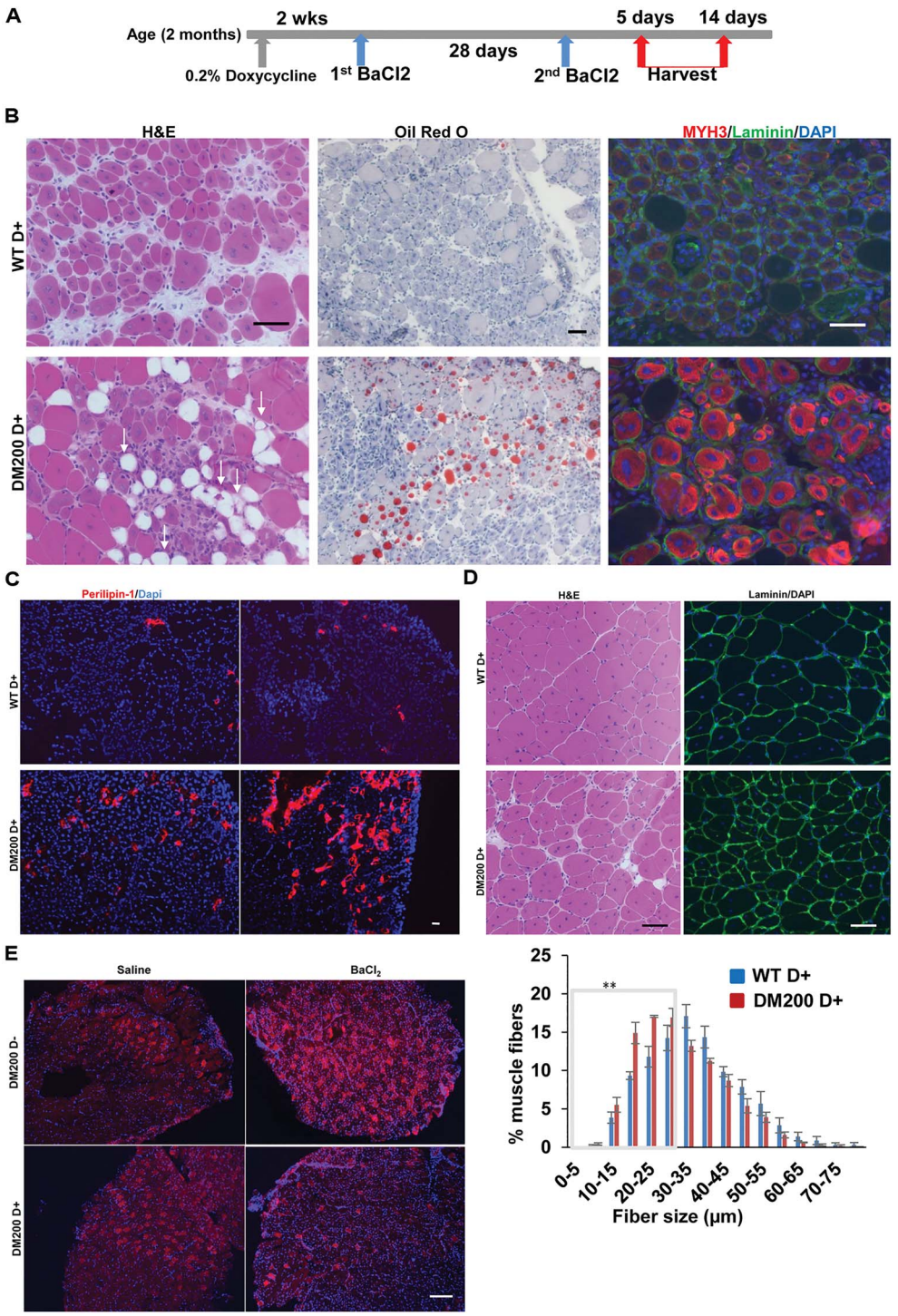

Figure 7. Repeated injury uncovers a dystrophic phenotype in skeletal muscles of RNA toxicity mice. (**A**) Schematic showing the experimental design used in this study. (**B**) H&E-stained sections of re-damaged TA muscles show increased fat droplets (white arrows) and a decreased number of regenerating fibers with persistent inflammatory response in DM200 D+ mice. Oil Red O staining confirms the increased presence of fat in TA muscles of DM200 D+ mice. MYH3 IF (an early fiber regeneration marker) (red) at 5 days post re-damage shows maturing fibers in wild-type mice (WT D+), while DM200 D+ mice show persistence of embryonic myosin expression. Laminin IF used for outlining muscle fibers (green), and nuclei stained with DAPI (blue). (**C**) IF for perilipin (a fat droplet surface marker) (red) shows increased adipogenesis in TA muscle sections from DM200 D+ mice as compared to WT D+ mice at 5 days post re-damage; nuclei are stained with DAPI (blue). (**D**) H&E staining and laminin IF (green) of TA muscle sections, with accompanying fiber size distribution quantification, show significantly smaller fibers in DM200 D+ mice as compared to WT D+ mice at 14 days post re-damage; $n = 3$ mice per group, $^{**}P < 0.01$, Student's t-test, error bars are mean ± SEM. (**E**) MYH2 IF (red) (a marker of fiber maturation) in TA muscle sections 14 days post re-damage ($BaCl_2$) shows decreased expression in DM200 D+ mice as compared to WT D+ mice. There was no difference in expression of MYH2 in non-injured muscle (saline) from the same DM200 D+ and WT D+ mice. Nuclei are stained with DAPI (blue). Scale bars = 50 μm.

regenerating fibers. We performed MYH3 IF as before, and it showed more MYH3 in the DM200D+ TA muscles as compared to the WT D+ TA muscles (Fig. 7B). At first, this was surprising, but the histology showed that the WT D+ mice had matured to the point where they were probably downregulating MYH3 expression, similar to what we had seen previously at 7 days post single damage (see Fig. 4C). These results suggested that beyond a defect in regeneration, there may also be issues with maturation of the regenerating muscle in the DM200 D+ mice. To evaluate this, we examined TA muscles collected at 14 days post damage. The H&E sections showed that almost all the muscle fibers in both the WT D+ and DM200D+ mice had central nuclei (Fig. 7D). This is consistent with the fact that we were looking at regenerating fibers from damaged areas in both cases. The WT D+ muscles showed a more organized distribution of fibers, whereas the DM200 D+ mice had more variability in fiber size, wider interstitial spaces (consistent with poorer maturation and increased deposition of collagen) and persistence of fat droplets. Fiber size analyses showed that the DM200 D+ mice had a significantly higher proportion of smaller muscle fibers (<30 microns diameter) ($P = 0.003$) (Fig. 7D). We then evaluated the expression of MYH2 in the muscles collected at 14 days post re-damage, using it as a marker of muscle fiber maturation (Fig. 7E). MYH2 is a fast myosin that is about 25% of the total myosin heavy chain expressed in mature adult mouse TA muscle. IF for MYH2 using an antibody specific for MYH2 showed that the saline-treated TA muscles in both DM200 D− and DM200 D+ mice had abundant and similar MYH2 expression, demonstrating that RNA toxicity did not have an overt effect on the expression of MYH2 in undamaged muscle. However, in the $BaCl_2$ damaged muscle, the TA muscle from DM200 D− mice showed robust expression of MYH2, whereas the TA muscles from DM200 D+ mice showed far fewer fibers expressing MYH2 (Fig. 7E and Supplementary Material, Fig. S8). This is consistent with delayed maturation of the damaged fibers in the presence of the toxic RNA.

Systemic ASO therapy corrects muscle regeneration defects caused by RNA toxicity

Recently, we showed that systemic treatment with an antisense oligonucleotide (ASO) targeted against the *DMPK* 3′UTR mRNA (ISIS 486178) was efficient in reversing key phenotypes of RNA toxicity such as myotonia, cardiac conduction defects and RNA splicing defects in the DM200 mouse model (44). Here, we aimed to test if ASO therapy was capable of having any beneficial effects on the adverse effects of RNA toxicity on satellite cells and muscle regeneration. To do this, we designed a treatment protocol for DM200 D+ mice, with the observers blinded to the treatment, wherein half of the cohort was treated with IONIS 877864 (h*DMPK*-ASO), a ligand-conjugated antisense (LICA-ASO), a 5′-palmitoyl-conjugated version of the ISIS 486178 (52,53). The other half was treated with another LICA-ASO, IONIS 885417 (control-ASO), a LICA control-ASO (Fig. 8A). We induced a cohort of 40 DM200 mice with doxycycline for 2 weeks. We confirmed that they had DM1 phenotypes by EMG and ECG (i.e. myotonia and cardiac conduction defects). Subsequently, half of them were administered IONIS 877864 subcutaneously (25 mg/kg twice a week) for 4 weeks, while the other half received the control-ASO. At the end of 4 weeks of treatment, the mice underwent the $BaCl_2$ damage in their right TA, while the left TA was injected with PBS. Tissues were collected at 5, 14 and 28 days post damage for evaluation of the effects on satellite cells and muscle regeneration. This protocol was repeated in a second cohort.

RNA-FISH confirmed that the number of RNA foci was reduced by IONIS 877864 in tissues collected from DM200 D+ mice at 5 days post damage (Supplementary Material, Fig. S9). H&E sections of TA muscles from 5 days post damage showed that the tissues from mice treated with IONIS 877864 had more regenerating fibers, whereas the tissues from mice treated with the control-ASO had persistence of the inflammatory infiltrate and fewer regenerating fibers (Fig. 8B). Fiber sizing confirmed that the mice treated with the h*DMPK*-ASO had larger central nucleated fibers with about 75% of them being greater than 20 microns diameter, as compared to only 30% with the control-ASO ($P = 0.004$) (Fig. 8C). MYH3 IF confirmed that the tissues from mice treated with IONIS 877864 had significantly larger regenerating fibers ($P = 0.01$) (Fig. 8D). Significantly, treatment with IONIS 877864 increased the number of PAX7+ve cells as compared to the control oligo ($P = 0.008$) (Fig. 8E). qRT-PCR found that the expression of the transgene was reduced by about 50% ($P = 0.00006$) by the IONIS 877864 ASO and that this was associated with a 50% increase in *Pax7* expression ($P = 0.024$) and a similar increase in *Myh3* expression ($P = 0.059$) (Fig. 9). Interestingly, there was significant reduction in the expression of *Col1a1* ($P = 0.026$), a gene associated with collagen synthesis. Overall, these results suggested that treatment with the h*DMPK*-ASO had a beneficial effect on muscle regeneration and satellite cells.

We extended our investigation to tissues collected at 14 and 28 days post damage. H&E histologic analyses of TA muscles collected at 14 days post damage suggested better resolution of damage in mice treated with IONIS 877864 as compared to the control-ASO (Fig. 10A and Supplementary Material, Fig. S10). Consistent with this, the fiber size analysis showed that the mice treated with the IONIS 885417 (control-ASO) trended ($P = 0.078$ for fibers size <25 μm) towards a smaller fiber size distribution (Supplementary Material, Fig. S11). In addition, the histologic analyses showed larger interstitial spaces in the TA muscles from mice treated with the control-ASO, suggesting increased collagen deposition. Gomori trichrome staining confirmed increased presence of collagen in the TA muscles of mice treated with the control-ASO as compared to mice treated with IONIS 877864 (Fig. 10B). Similar results for H&E and Gomori trichrome staining were seen in TA muscles collected 28 days post damage (Fig. 10C and Supplementary Material, Fig. S12). qRT-PCR showed that the transgene GFP mRNA levels were significantly less ($P = 0.049$) in the h*DMPK*-ASO treated TA muscles as compared to mice treated with the control-ASO (Fig. 11A). Interestingly, this time point, 28 days post damage, is 4 weeks after the last dose of ASO treatment and is a reflection of the duration of its therapeutic effect. The decrease in toxic RNA levels was associated with a significant increase ($P = 0.043$) in *Pax7* mRNA levels (Fig. 11A). Importantly, this was also associated with a significant rescue in the number of PAX7+ve cells ($P = 0.0002$) in the h*DMPK*-ASO treated muscles to the levels found in TA muscles from wild-type mice that had undergone the 28-day damage protocol (Fig. 11B).

Discussion

DM1 is the most common muscular dystrophy disorder in adults. It is a progressive dystrophy happening over decades and so is typically much slower than that seen in Duchenne muscular dystrophy. Practically, it has thus been difficult to characterize the muscular dystrophy and elements contributing to the pathogenesis, from a clinical perspective. Many mouse models of RNA

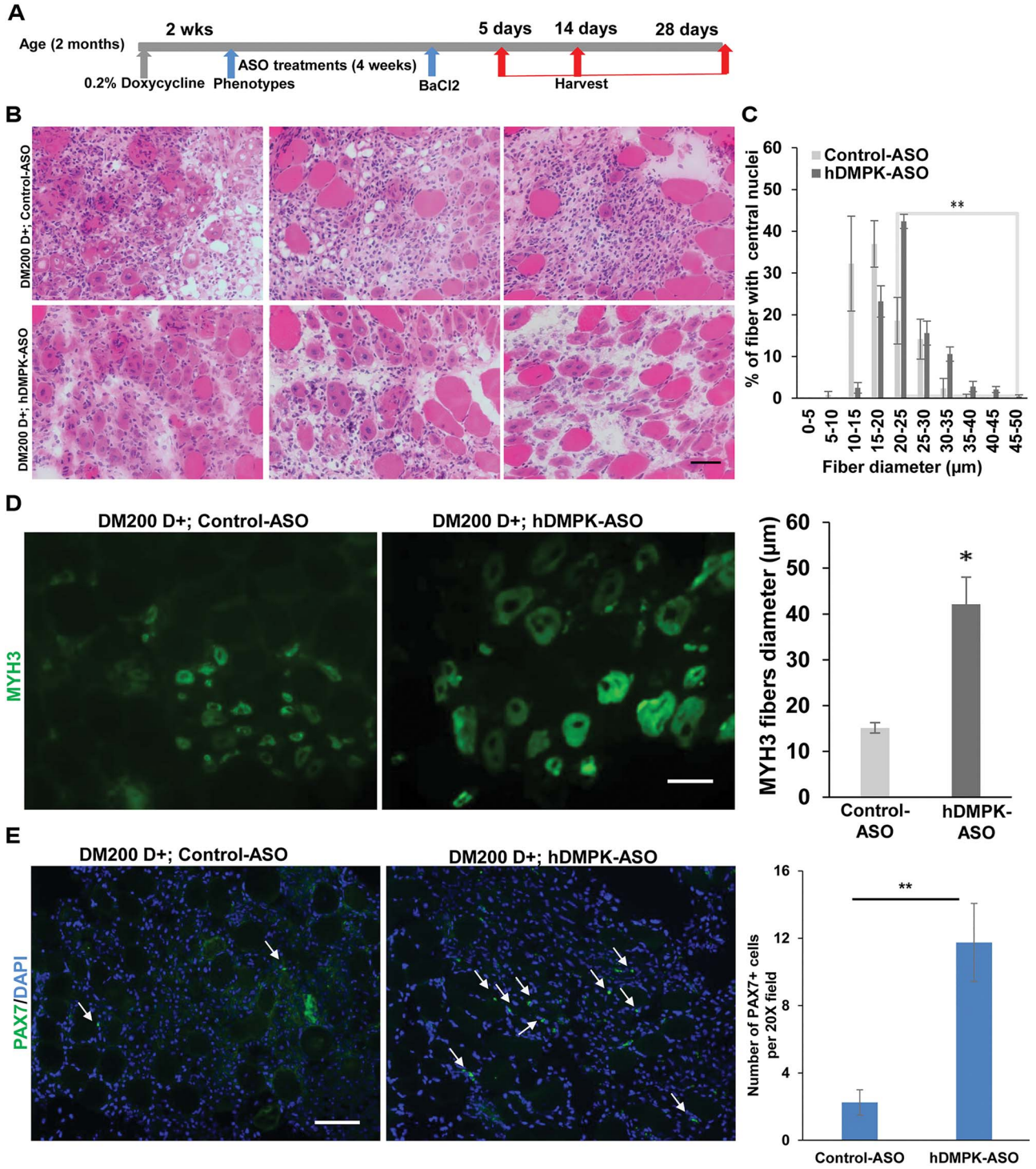

Figure 8. LICA-ASO treatment improves muscle regeneration in RNA toxicity mice. (**A**) Schematic showing the experimental design used in this study. (**B**) H&E staining of TA muscle sections and (**C**) fiber size analysis show significantly increased size of central nucleated fibers (i.e. regenerating fibers) in h*DMPK*-ASO (IONIS 877864) treated mice as compared to control-ASO treated mice at 5 days after injury; $n = 4$ mice per group, $^{**}P < 0.01$, Student's *t*-test, error bars are mean ± SEM. H&E sections also show better resolution of inflammatory response and reduced fat droplets with h*DMPK*-ASO treatment. (**D**) IF for MYH3 (green) in TA muscle sections shows increased expression of MYH3 and larger size of regenerating fibers in h*DMPK*-ASO treated mice as compared to control-ASO treated mice at 5 days post injury; graph showing fiber size quantification of MYH3 positive fibers; $n = 3$ mice per group; $^{*}P < 0.05$; Student's *t*-test; error bars are as mean ± SEM. (**E**) IF for Pax7 (green) in TA muscle sections shows increased number of PAX7+ve cells (white arrows) in h*DMPK*-ASO treated mice as compared to control-ASO treated mice at d5 after injury. The graph shows number of PAX7+ve cells per 20× field; $n = 4$ mice per group; five non-overlapping fields/mouse; $^{**}P < 0.01$; Student's *t*-test; error bars are as mean ± SEM. Nuclei are stained with DAPI (blue). Scale bars = 50 μm.

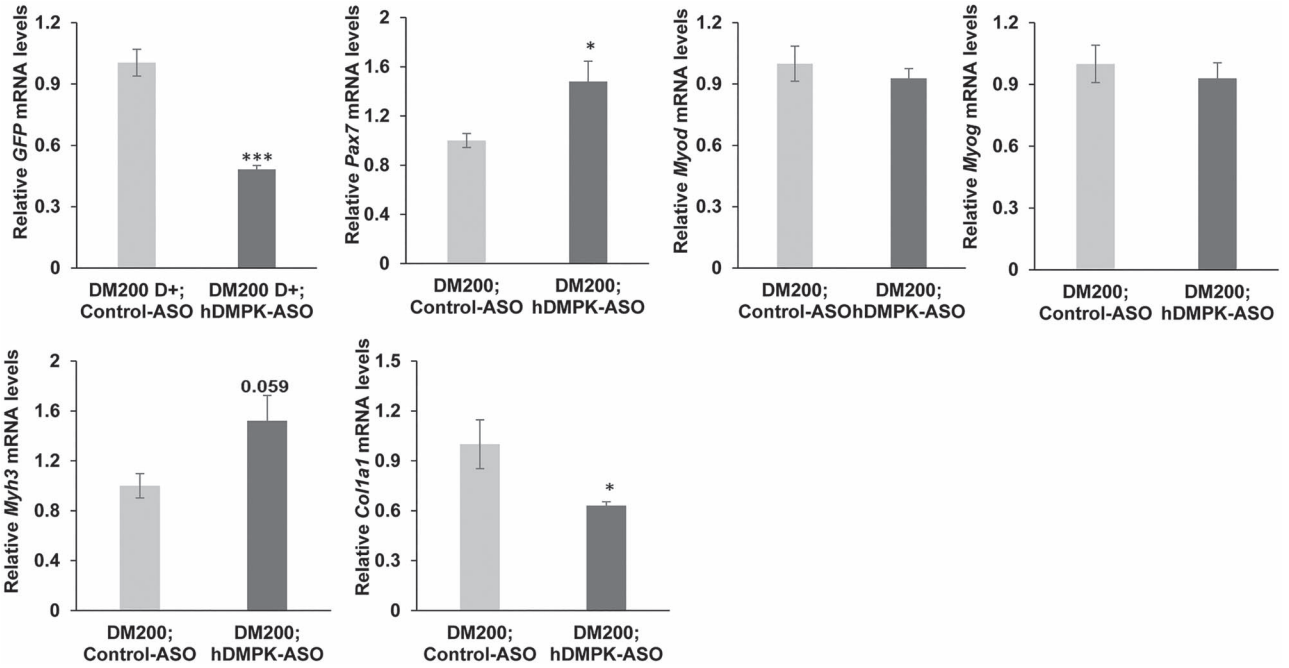

Figure 9. Gene expression analyses with h*DMPK*-ASO treatment. qRT-PCR from TA muscles collected 5 days post $BaCL_2$ injury shows that the h*DMPK*-ASO reduced toxic RNA levels (*GFP DMPK* 3′UTR mRNA) in DM200 D+ mice as compared with mice treated with the control-ASO. qRT-PCR also shows increased expression of *Pax7* (marker of satellite cells) and *Myh3* (regeneration marker). There was no significant difference in the expression of *Myod* or *Myog*. qRT-PCR also shows significant decreased expression of *Col1a1* mRNA (a marker of fibrosis). $n = 4$–5 mice per group; $^{*}P < 0.05$, $^{***}P < 0.001$; Student's *t*-test; error bars are mean ± SEM.

toxicity have been generated to study the concept of RNA toxicity and its role in DM1 (5). However, most have limited evidence for progressive dystrophic changes, including the prototypic HSA-LR mouse model (54). This is true of the DM200 mouse model presented here as well, where we do not observe significant weight loss, loss of muscle mass or muscle fiber size changes (Supplementary Material, Fig. S5) in the 1- to 2-month window of the studies (44). Other studies have reported some evidence for dystrophic changes in the homozygotes of the DMSXL mouse model, which express the CUG expanded *DMPK* mRNA from a transgene encoding the entire human gene with $(CTG)_{>1000}$ (55). However, this model has severe growth retardation (body weight of only 50% of wild-type littermates) and very high pre-weaning mortality (>60%), complicating the study of muscle wasting and dystrophy. More recently, another mouse model, the TREDT960I, containing a tetracycline inducible transgene with human *DMPK* exons 11–15 with a 960 interrupted CTG repeat, has been reported to have gender specific mild myopathic changes in specific muscles in the absence of regeneration (8). Of note, with the exception of the DMSXL mouse model (55), the remaining mouse models have robust expression of the toxic RNA, with levels that are significantly higher than the *Dmpk* gene (8,45). This suggests the possibility that the threshold for toxicity in mouse skeletal muscles leading to dystrophic changes is higher or that other unknown or differing mechanisms may be at play between the mouse and human conditions.

Here, we decided to use a controlled experimental approach to elicit skeletal muscle damage and study the regenerative response to it. Although, this may not be the typical way in which muscle damage is likely to occur in the human condition, the concept of chemically (cardiotoxin, notexin, $BaCl_2$) or physically (freeze injury) induced damage has been used for several decades to define the underlying molecular, cellular and histologic changes that happen during the regenerative response to damage (13,16,47–49). The key to a regenerative response in adult skeletal muscle is the satellite cell. Several elegant studies using genetically modified mice have clearly shown that satellite cells are indispensable to adult muscle regeneration (50,56–58). Severe reductions in the number of satellite cells resulted in impaired regeneration and increased fibrotic and fatty infiltration with repeated damage.

Satellite cells are found between the basal lamina and the sarcolemma of muscle fibers and constitute between 2 and 10% of myonuclei depending on the muscle and organism. Satellite cells stay in a quiescent state and are activated by physiological growth and physical activity. In damaged muscles, they are activated by a number of cytokines and growth factors released by inflammatory cells responding to damage. They are characterized by the expression of PAX7, a paired box transcription factor. With respect to DM1, it is not clear if *DMPK* is expressed in satellite cells *in vivo*. Our analysis found that satellite cells do have the RNA foci associated with mutant *DMPK* mRNA (Fig. 1). We also evaluated our DM200 mouse model for the presence of RNA foci in PAX7+ve cells and found that they too have RNA foci in satellite cells *in vivo*. The transgene in the DM200 mice is driven by the putative human *DMPK* promoter (43,59); and its expression in other tissues such as skeletal muscle, the heart and smooth muscles (43) is consistent with endogenous *Dmpk* expression. Our data along with those from iPSC cells support the idea that *DMPK* is expressed in satellite cells. Since MBNL1 co-localizes with RNA foci and is reported to be necessary for RNA foci formation (40), we also looked for MBNL1 expression in satellite cells. We saw evidence for MBNL1 in satellite cells in muscles tissues from human and mouse and for possible sequestration of MBNL1. In addition, we found evidence for MBNL2 expression in murine satellite cells.

It is clear from our data that RNA toxicity in the DM200 mice leads to decreased PAX7+ve cells (satellite cells). Uninduced

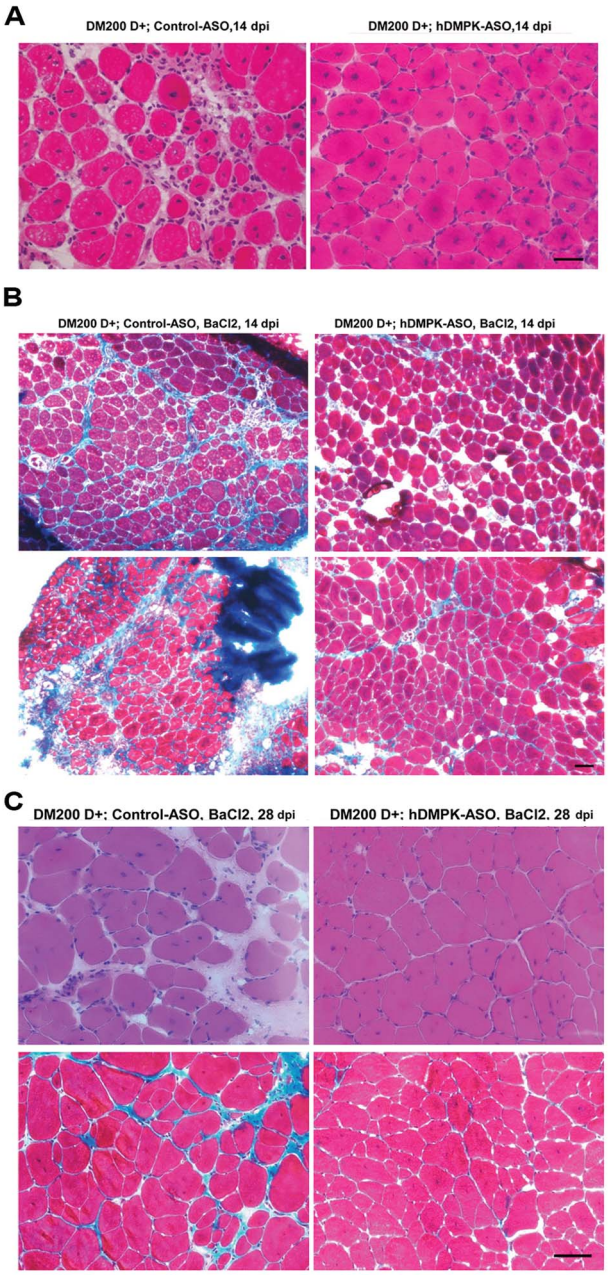

Figure 10. LICA-ASO improves muscle regeneration and reduces dystrophic changes in RNA toxicity mice. (**A**) H&E staining of TA sections shows improved muscle histology in DM200 D+ mice treated with h*DMPK*-ASO as compared with control-ASO at 14 days post injury (dpi). Scale bar = 20 μm. (**B**) Gomori trichrome staining of representative TA muscle sections collected at 14 dpi shows decreased collagen staining (blue stain) in the h*DMPK*-ASO-treated DM200 D+ mice as compared to control-ASO treated mice. (**C**) Representative images of H&E staining and Gomori trichrome staining of TA muscle sections collected at 28 dpi from DM200 D+ mice treated with either control-ASO or h*DMPK*-ASO show decreased fibrosis and more intact muscle architecture in the h*DMPK*-ASO-treated mice. For B and C, scale bars = 50 μm.

DM200 mice, which express the transgene RNA due to some transgene leakiness, in the absence of doxycycline induction, have decreased *Pax7* expression by about 50% (Fig. 2). However, the number of satellite cells in the TA or quadriceps muscles did not differ from that found in wildtype mice (Supplementary Fig. S4). This suggests that in the DM200 D− mice that the reduction in *Pax7* mRNA levels may be due to decreased expression of the gene in satellite cells and not due to loss of satellite cells. However, when we induced the DM200 mice with doxycycline, this resulted in a further progressive decease in *Pax7* mRNA levels starting as early as 5 days post induction (Fig. 2). By 1 week post induction, the levels were approximately 20% of those found in wild-type mice. Coinciding with this reduction in expression of *Pax7* in the DM200 D+ mice, we found decreased numbers of satellite cells by 2 weeks post induction (Fig. 3 and Supplementary Material, Fig. S4). This is not due to doxycycline as we did not see any effect of doxycycline on satellite cell numbers or *Pax7* expression in wild-type mice (Supplementary Material, Fig. S3). We also noted, though this was difficult to quantify, that the signal intensity from PAX7-IF seemed diminished in the PAX7+ve cells in the skeletal muscles of DM200 D+ mice. Though speculative, it may be that there could be a threshold level of PAX7 expression for satellite cell maintenance or function (60). We performed TUNEL assays (for apoptosis) as well as IF assays for Ki67 (a marker of cellular proliferation) to assess if there was evidence of increased apoptotic activity or changes in cellular proliferation in the TA muscles. We saw scant evidence for any apoptosis or proliferation, and there were no differences between DM200 D+ mice and wild-type mice (data not shown).

PAX7 is required for satellite cell specification (14) and is universally used as the marker for satellite cells. In a series of elegant and complementary experiments, satellite cells were shown to be indispensable for muscle regeneration in adult mice (50,56–58,61). So, we used an injury model ($BaCl_2$ intramuscular injection) to assess if the reduction in satellite cells had any functional consequences with respect to muscle regeneration in DM200 mice with RNA toxicity. Our results clearly show that there is a defect in muscle regeneration as measured by a variety of parameters including MYH3 expression, *MyoD* and *Myog* expression, fiber size and satellite cell response to damage (see Figs 3–6). Furthermore, even after waiting for 56 days, we saw a persistence of smaller fibers and significantly reduced satellite cell numbers in the DM200 D+ mice (Fig. 6). These experiments demonstrate a delay in regenerative response, a lack of muscle fiber maturation and an inability to maintain a normal number of satellite cells.

One of the things that the inability to maintain the satellite cell pool predicts is that the consequences of repeated damage may be more severe. This has been borne out by previous studies in which repeated instances of induced damage resulted in further impairment in the repair response and the elicitation of a more dystrophic phenotype with increased fat droplet infiltration and an increased fibrotic response (50,56,57,62). In the DM200 model, this is exactly what we see. With a second episode of induced damage, the DM200 D+ mice show increased fat droplets in the damaged muscle and a reduction in the number of regenerating fibers (Fig. 7B and C and Supplementary Material, Fig. S7A and B). The histology and fiber sizing showed smaller fibers and increased fibrosis (Fig. 7D), while the MYH2 analysis showed clear evidence of decreased fiber maturation at this stage of repair (Fig. 7E and Supplementary Material, Fig. S8). In total, all of these results are consistent with a dystrophic phenotype being brought out by repeated muscle damage. This is one of the first times to model these classic markers of dystrophic changes (i.e. fat deposition and fibrosis) in the skeletal muscles of a mouse model of RNA toxicity. Though such changes are typically reported in muscles of patients with Duchenne muscular dystrophy, they

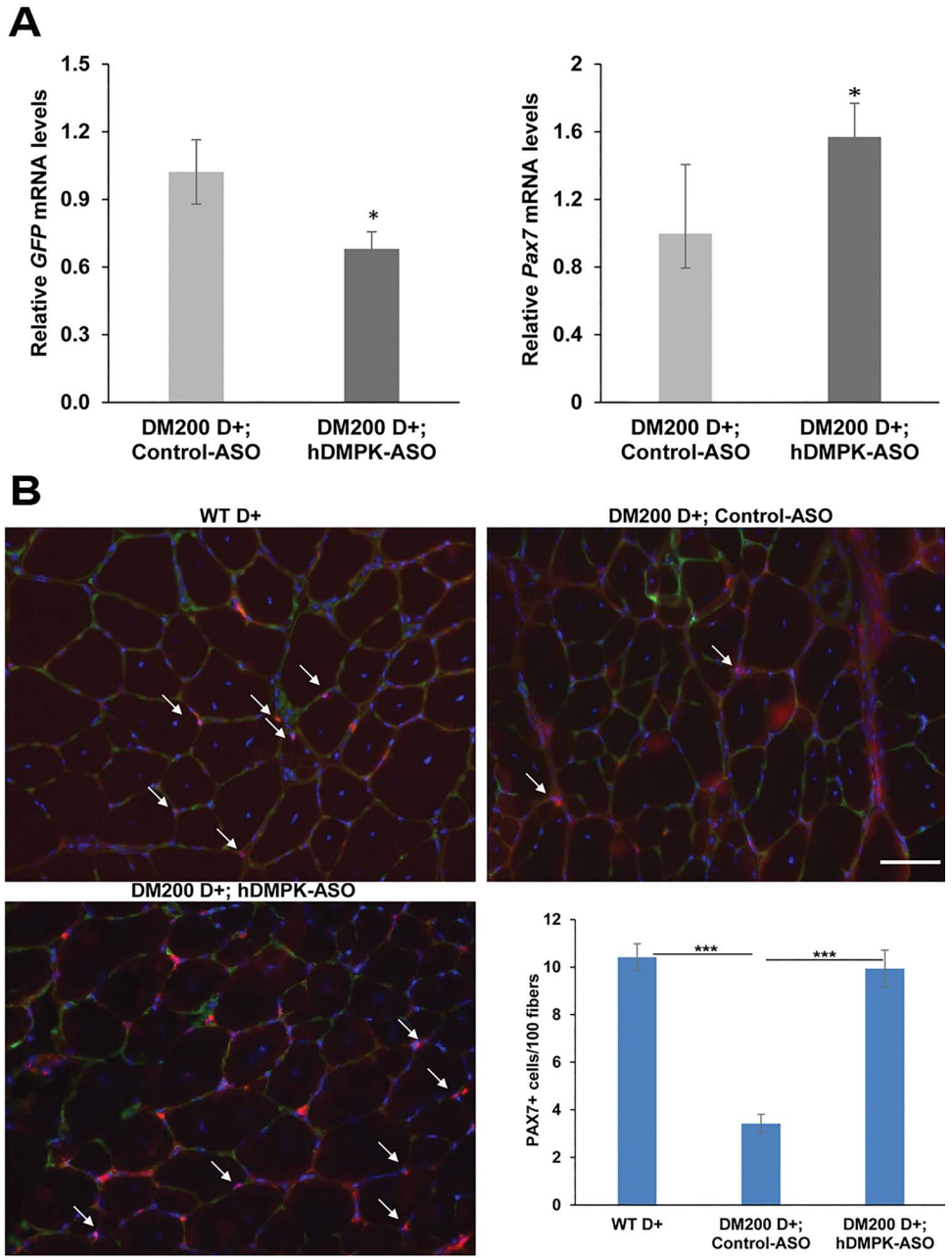

Figure 11. LICA-ASO treatment rescues satellite cells in the RNA toxicity mouse. (**A**) qRT-PCR shows decreased expression of toxic RNA (*GFP DMPK* 3′UTR mRNA) and increased *Pax7* mRNA in TA muscles of DM200 D+ mice treated with h*DMPK*-ASO as compared with control-ASO treated mice, at 28 dpi. $n = 4$–5 mice per group, $^{*}P < 0.05$; Student's *t*-test, error bars are mean ± SEM. (**B**) IF for PAX7 (red) and quantification of satellite cells (white arrows) in TA muscle sections collected at 28 dpi show that treatment with h*DMPK*-ASO rescued the defect in satellite cell number caused by RNA toxicity; compare WT D+ to DM200 D+ mice treated with control-ASO or h*DMPK*-ASO. Nuclei are stained blue with DAPI. $n = 4$–5 mice per group; 3–5 non-overlapping sections/mouse; $^{***}P < 0.001$; Student's *t*-test; error bars are as mean ± SEM. Scale bars = 50 µm.

are also seen in the skeletal muscles of patients with DM1 (Supplementary Material, Fig. 13). Recent studies using MRI have found increased fat infiltration in truncal muscles of patients with DM1 that correlated with decreased strength (63). Other studies found that more than 70% of DM1 patients had MRI evidence of fatty infiltration in their lower limb muscles and that this correlated with clinical measures of muscle function (64–67).

Having established a model of muscle regeneration defects due to RNA toxicity, we sought to determine if these would be amenable to therapeutic intervention. Recently, we published a study demonstrating the utility of systemic ASO therapy targeting the *DMPK* 3′UTR in reversing multiple phenotypes in the DM200 RNA toxicity model. This included myotonia, cardiac conduction defects and RNA splicing defects, all of which coincided with a reduction in the levels of the toxic RNA and in a reduction in RNA foci in affected tissues. Here, we utilized a fatty acid ligand-conjugated version of the ASO that was used in the previous study. This palmitoyl-conjugated ASO is about 3–4 times more potent than the ISIS 486178 ASO we used in

our previous study (52,53). To our knowledge, this is the first time that a LICA-ASO targeting the *DMPK* 3′UTR has been used in a mouse model of RNA toxicity. We treated the mice for 4 weeks, with twice weekly, subcutaneous administration of the ASO based on data gathered from prior studies (52,53). Of note, this ASO (IONIS 877864) and the duration of treatment were effective in reducing the number of RNA foci in the TA muscles of treated mice (Supplementary Material, Fig. S9). The mice treated with the ASO also had better muscle regeneration after induced damage, as early as 5 days post damage, based on H&E histology, fiber sizing and MYH3 expression (Fig. 8). Notably, at this time point, the treatment had also increased the number of satellite cells in response to damage, as compared to the control-ASO (Fig. 8E). This coincided with increased *Pax7* expression (Fig. 9). By 14 days post damage, H&E staining, fiber sizing and Gomori staining also showed larger fibers and decreased collagen deposition in the IONIS 877864 treated mice, and this persisted to the end of the experiment at 28 days post damage (Fig. 10). At this time point, the mice treated with the IONIS 877864 ASO showed almost complete resolution of the damage with minimal fibrotic changes in contrast to the control-ASO mice, which showed significant fiber size variability and clearly evident fibrosis (Fig. 10D). Importantly, at this time point, the LICA-ASO treatment also restored the satellite cell numbers in the DM200 D+ mice to those found in wild-type mice (Fig. 11). These results show that muscle regeneration defects and muscular dystrophy phenotypes such as fibrosis may be amenable to systemic ASO therapy. The results also show that such therapy may be also able to correct the reduction in satellite cell numbers.

Satellite cells have typically been studied in the context of their role in muscle regeneration. Over the past decade, the research team at the Center for Muscle Biology at the University of Kentucky has done a series of elegant studies using a novel mouse strain in which diphtheria toxin is expressed conditionally in *Pax7* expressing cells to deplete satellite cells by about 90% (61). With this mouse strain, they were one of the groups to show the indispensable requirement for satellite cells for muscle repair in response to damage in adult mice. Over the last decade, they have also demonstrated other roles for satellite cells in adult muscle. They have reported on the role for satellite cell depletion in the accumulation of the extracellular matrix and fibroblast expansion in skeletal muscle (68–70). They also reported a potential role for satellite cells in maintaining proper muscle spindle fiber function and gross motor coordination (71). This was associated with decreased wheel running performance and lipid accumulation in the skeletal muscle. Furthermore, they showed that satellite cell depletion in adult mice was associated with altered muscle morphology in chronically stretched muscle and that this was associated with smaller muscle fibers and increased fibrosis (72). More recently, they have shown that satellite cell depletion has a deleterious effect on physical function and muscle fiber hypertrophy in exercised, physically active mice (73). Altogether, these studies provide a strong base of evidence for the role of satellite cells in adult muscle that goes beyond the indispensable role in the regenerative response in damaged muscle. Though speculative, it might be interesting to study the role of reduced satellite cells in other functional and histologic aspects of DM1 pathology.

The toxic RNA clearly has deleterious effects on satellite cell numbers. Unfortunately, we have yet to resolve how this happens. Our preliminary analyses do not show evidence of increased apoptosis or proliferation changes in the skeletal muscles of the DM200 D+ mice. Admittedly, though it would have been difficult to capture a satellite cell in the active process of apoptosis, we did not see such events. Additional experiments in the future, using single fiber analysis in culture, or satellite cell marker mice may be able to address this. Another possibility is that a threshold level of PAX7 expression is required to maintain a satellite cell. In the uninduced DM200 mice (DM200 D−), the *Pax7* expression levels were already reduced to about 50% of that in wild-type mice (Fig. 2). At this level of expression, there was no reduction in satellite cell numbers (Supplementary Material, Fig. S4). However, upon induction of the transgene, we saw further reductions in *Pax7* expression such that it was about 20% of the levels found in wild-type mice by 1 week post induction. This coincided with a dramatic decrease in the satellite cell number (Fig. 2 and Supplementary Material, Fig. S4). It has been proposed that an inhibitory circuit exists between PAX7 and myogenic regulatory factors, namely MyoD and myogenin (74,75). In this model, high PAX7 levels repress MyoD through effects on MyoD protein stability and *Myod* transcription and that the onset of myogenin expression, which is downstream of MyoD activation, represses PAX7. This model also predicts that lower levels of PAX7, below a certain threshold, would result in increased MyoD activity and precocious differentiation of the satellite cell and thus result in a decreasing satellite cell pool (and decreasing *Pax7* mRNA levels). Interestingly, we found that *MyoD* mRNA levels were increased significantly ($P = 0.04$) in the DM200 D− mice (Fig. 2). This was associated with a 2-fold increase in *Myog* mRNA levels in DM200 D− mice that increased up to 4.5-fold by 4 days after doxycycline induction of the transgene (Fig. 2). This coincided with decreasing *Pax7* expression (Fig. 2). Thus, our data are consistent with the proposed model. Altogether, these findings suggest that the reduction in satellite cells may be due to precocious differentiation of those cells. To this end, the Rudnicki Lab published an elegant study using a tamoxifen-inducible PAX7 depletion model (50), which showed in cell culture studies using cultured myofibers that reducing PAX7 resulted in decreased proliferation without evidence of apoptosis and increased expression of myogenin, suggesting precocious differentiation. They also used this mouse model to study the *in vivo* effects of PAX7 depletion. They found that reductions in PAX7+ve cells to about 20% of normal (similar to reductions seen in DM200 D+ mice; see Fig. 2), led to impaired regeneration and increased expression of fat droplets and fibrotic tissue in response to induced muscle damage and repeated damage. In fact, their mouse model is remarkable for how well the phenotypes match the results from our current study in the DM200 mice.

The effects on satellite cells may also be a non-cell autonomous effect (16,74,76). The satellite cell exists in its special niche closely associated with a myofiber, blood vessels, nerves and different surrounding cells such as fibroadipogenic cells (FAPs), fibroblasts, pericytes, etc. In a damaged muscle, this milieu becomes even more complex with the addition of macrophages, lymphocytes, eosinophils and other inflammatory cells. Many of these cells express cytokines, growth factors and extracellular matrix proteins that can alter satellite cell numbers and function as well. Temporal regulation of the complex events that happen during muscle regeneration is important for proper repair. For instance, persistence of the inflammatory state in damaged muscle could result in an aberrant cytokine milieu that is deleterious to satellite cell maintenance or expansion in response to damage. Similar effects could happen on support cells such as the FAPs, which have been shown to have beneficial effects on satellite cell

function in myogenesis in early stages of muscle regeneration (77,78). But, in chronic damaged states, this can lead to deleterious effects on satellite cell pool maintenance (79–81). FAP cells are considered to be the principal mediators of fatty and fibrous tissue accumulation in muscular dystrophy (82). Recent studies have shown the importance of FAP cells in the pathology underlying muscular dystrophies and the potential for beneficial therapeutic intervention targeting these cells in Duchenne muscular dystrophy (83) and limb girdle muscular dystrophy 2B (84). It is notable that the products of excessive FAP activity, namely increased adipogenesis and fibrosis in skeletal muscle, are exactly what we see in the DM200 mouse model with repeated injury. The role of FAP cells in RNA toxicity and DM1 warrants further exploration.

In summary, our studies find that RNA toxicity caused by the mutant *DMPK* 3′UTR mRNA clearly leads to defects in muscle regeneration, deficits in satellite cell numbers and elicits a dystrophic phenotype with repeated damage. Importantly, the IONIS 877864 ASO treatment and its efficacy showed clearly that the defects in regenerative response to damage and the defects in satellite cell numbers in the DM200 mouse model are due to the toxic RNA. It is difficult to attribute these phenotypes to doxycycline, an insertional effect from the transgene on some other gene, etc. The effect of the ASO is specific to the targeting of sequences found within the *DMPK* 3′UTR in the toxic RNA expressed from the transgene. From a clinical perspective, the ASO treatment also demonstrates the possibilities for therapeutic interventions to mitigate the muscular dystrophy associated with RNA toxicity in DM1.

Materials and Methods

Experimental mice and ASOs

The DM200 mouse model expresses a GFP-*DMPK* 3′UTR $(CTG)_{200}$ transgene under the control of the human *DMPK* promoter upon induction with doxycycline (43,44). The transgenic mice were induced with 0.2% doxycycline in drinking water at the age of 2 months. For mice induced with doxycycline, phenotyping using EMG and ECG was performed as previously described, at 2 weeks post induction, to confirm the presence of DM1 phenotypes (43,44). DM200 D+ mice were maintained on doxycycline through the duration of experiments.

For experiments involving ASOs, we used ligand-conjugated antisense oligonucleotides (LICA-ASOs) that were provided to us by IONIS Pharmaceuticals, Carlsbad, CA. These LICA-ASOs were palmitoyl-conjugated gapmers (52,53): IONIS 877864 (5′-**ACA**ATAAATACCG**AGG-**3′; cEt 2′ sugar modification), which targets a region in the *DMPK* 3′UTR distal to the CUG repeats, and a control-ASO, IOsNIS 885417 (5′-GGCCAATACGCCGTCA-3′; cEt 2′ sugar modification). As described above, we performed phenotypic analyses of DM200 D+ mice at 2 weeks post induction to confirm the presence of DM1 phenotypes in the mice. We then treated the mice in a blinded fashion for our studies. We dissolved the oligonucleotides in PBS and administered at a dose of 25 mg/kg by subcutaneous injections, twice a week for 4 weeks. All animals were used in accordance with protocols approved by the Animal Care and Use Committee at the University of Virginia. DM200 D+ mice were maintained on doxycycline throughout the course of the experiments.

Muscle regeneration

For induced muscle damage, 100 µl of 1.2% $BaCl_2$ (Sigma-Aldrich, St. Louis, MO) dissolved in saline was injected into the right TA muscle of mice to induce necrotic injury. The TA muscle in the opposite leg of each mouse was injected with PBS as a control. For the double injury protocol, we injected a repeat dose of $BaCl_2$ or PBS into the corresponding TA muscles 28 days after the first injury. Mice were euthanized and TA muscles were harvested at various time points as indicated in the Results section.

H&E, Gomori trichrome and Oil Red O staining of skeletal muscles

H&E staining was performed according to standard protocols. Collagen was detected using a Gomori trichrome stain [#87020, Thermo Scientific™ Richard-Allan Scientific™ Gomori Trichrome (Blue Collagen), Waltham, MA]. Oil Red O (O1391, Sigma-Aldrich) staining was performed according to manufacturer's protocols to visualize oil droplets. At least three non-overlapping sections per mouse were analyzed and 3–5 mice per group were analyzed.

Muscle fiber sizing and counting of fibers with central nuclei

Muscle fiber sizing was done using CarlZeiss AxioVision™ (Germany) software by measuring the cross-sectional area of each muscle fiber in digital images of H&E stained skeletal muscle (TA) sections captured at 200× magnification. Counting of fibers was also done using the same software. At least three non-overlapping sections per mouse were analyzed and 3–5 mice per group were analyzed.

RNA-FISH and IF

For RNA-FISH, tissue was fixed in 4% paraformaldehyde in 1× PBS and a Cy3-CAG10 (Integrated DNA technologies, IDT, Coralville, IA) probe used for hybridization. Details about the RNA-FISH and IF protocols are described elsewhere (85). Primary antibodies were anti-PAX7 [1:50, Developmental Studies Hybridoma Bank (DSHB, Iowa City, IA)], anti-MBNL1 (1:1000, A2764, gift from Dr Charles A. Thornton), anti-MBNL2 [1:500, SC136167 (clone 3B4), Santa Cruz Biotech, Dallas, TX], anti-MYH3 (1:200, clone F1.652, DSHB), anti-laminin (1:1000, catalog L9393, Sigma-Aldrich), anti-Perilipin (1:500, #9349, Cell Signaling Technology, Danvers, MA) and anti-MYH2 (1:100, SC-71-c, DSHB). Secondary antibodies were from Molecular Probes, Eugene, OR (1:1000 dilution). For quantification of PAX7+ cells, at least three non-overlapping sections per mouse were analyzed and 3–5 mice per group were analyzed.

RNA isolation and qRT-PCR assays

We extracted total RNA from skeletal muscle tissues using published protocols (86). All RNAs are DNAse treated and confirmed to be free of DNA contamination. QuantiTech™ Reverse Transcription Kit (Qiagen™, Germantown, MD) was used for making cDNA from 1 µg of total RNA. qRT-PCR was done using the BioRad iCycler™ (Biorad, Hercules, CA) and detected with SYBER™ Green dye. Data were normalized using an endogenous control (*Gapdh*), and normalized values were subjected to a $2^{-\Delta\Delta Ct}$ formula to calculate the fold changes between uninduced and induced groups. Primer sequences are given in Supplementary Material, Table S1. As a quality control, if the *Gapdh* threshold cycle (Ct) in real-time RT-PCR was greater than 20 cycles, the RNA was re-extracted from the tissue. At least 3–5 mice were analyzed for each data point and each specimen for each data point was analyzed in duplicate. For quality control,

if the Ct between duplicates was greater than 0.5 cycles, the real-time PCR was repeated for that sample. If a sample or target had a Ct $\geq$ 35 cycles, these were considered as below the detection limit and not included in further analyses.

Statistical analysis

Standard statistical methods were employed. Briefly, data sets were first analyzed for outliers using the Grubb's test, also known as the ESD method (extreme studentized deviate). For real-time PCR, outliers were assessed prior to calculation of fold change. Once outliers were removed, the data set was analyzed for normality. If normal, two-tailed Student's *t*-tests were employed to assess significance, with attention paid to equal versus unequal variance as appropriate. ANOVA analysis (Tukey multiple comparison) was used if appropriate. If the data set was non-normal, the Mann–Whitney assessment for statistical significance was used. Minitab® 16.1.0 (Minitab, Inc., State College, PA) and Microsoft Excel were the software used. All data are expressed as mean $\pm$ SEM. $^{*}P < 0.05$, $^{**}P < 0.01$, $^{***}P < 0.001$ (Student's *t*-test). $P < 0.05$ was considered statistically significant unless otherwise specified.

Supplementary Material

Supplementary Material is available at *HMG* online.

Acknowledgements

C.F.B. is an employee and shareholder in Ionis Pharmaceuticals Inc. and an inventor on patent #WO201502457A3 regarding ISIS 486178 antisense technology for modulation of *DMPK* expression. F.R. is an employee and shareholder in Ionis Pharmaceuticals Inc. We would like to thank Dr C. Thornton and Dr M. Nakamori for tissue samples from individuals with DM1.

Conflicts of Interest statement. None declared.

Funding

This work is supported by the National Institutes of Health (grant R01AR071170) and the generosity of the Stone Circle of Friends.

Authors' contributions

M.S.M. did experimental design, microscopy, phenotyping and wrote the manuscript. R.S.Y. co-wrote the manuscript, did experimental design and experiments on RNA-FISH, splicing and expression analyses. M.M. designed and did phenotyping in concert with M.S.M. M.M. and R.S.Y. did expression analyses. J.M.G., M.M. and R.S.Y. did fiber sizing analyses and microscopy. F.R. and C.F.B. provided ASOs for the study and helped in the design and implementation of the blinded studies of the ASOs and evaluation and editing of the manuscript.

References

1. Day, J.W. and Ranum, L.P. (2005) RNA pathogenesis of the myotonic dystrophies. *Neuromuscul. Disord.*, **15**, 5–16.
2. Mahadevan, M., Tsilfidis, C., Sabourin, L., Shutler, G., Amemiya, C., Jansen, G., Neville, C., Narang, M., Barcelo, J., O'Hoy, K. *et al.* (1992) Myotonic dystrophy mutation: an unstable CTG repeat in the 3′ untranslated region of the gene. *Science*, **255**, 1253–1255.
3. Taneja, K.L., McCurrach, M., Schalling, M., Housman, D. and Singer, R.H. (1995) Foci of trinucleotide repeat transcripts in nuclei of myotonic dystrophy cells and tissues. *J. Cell Biol.*, **128**, 995–1002.
4. Echeverria, G.V. and Cooper, T.A. (2012) RNA-binding proteins in microsatellite expansion disorders: mediators of RNA toxicity. *Brain Res.*, **1462**, 100–111.
5. Braz, S.O., Acquaire, J., Gourdon, G. and Gomes-Pereira, M. (2018) Of mice and men: advances in the understanding of neuromuscular aspects of myotonic dystrophy. *Front. Neurol.*, **9**, 519.
6. Jones, K., Wei, C., Iakova, P., Bugiardini, E., Schneider-Gold, C., Meola, G., Woodgett, J., Killian, J., Timchenko, N.A. and Timchenko, L.T. (2012) GSK3beta mediates muscle pathology in myotonic dystrophy. *J. Clin. Invest.*, **122**, 4461–4472.
7. Kuyumcu-Martinez, N.M., Wang, G.S. and Cooper, T.A. (2007) Increased steady-state levels of CUGBP1 in myotonic dystrophy 1 are due to PKC-mediated hyperphosphorylation. *Mol. Cell*, **28**, 68–78.
8. Morriss, G.R., Rajapakshe, K., Huang, S., Coarfa, C. and Cooper, T.A. (2018) Mechanisms of skeletal muscle wasting in a mouse model for myotonic dystrophy type 1. *Hum. Mol. Genet.*, **27**, 2789–2804.
9. Yadava, R.S., Foff, E.P., Yu, Q., Gladman, J.T., Kim, Y.K., Bhatt, K.S., Thornton, C.A., Zheng, T.S. and Mahadevan, M.S. (2015) TWEAK/Fn14, a pathway and novel therapeutic target in myotonic dystrophy. *Hum. Mol. Genet.*, **24**, 2035–2048.
10. Yadava, R.S., Foff, E.P., Yu, Q., Gladman, J.T., Zheng, T.S. and Mahadevan, M.S. (2016) TWEAK regulates muscle functions in a mouse model of RNA toxicity. *PLoS One*, **11**, e0150192.
11. Heatwole, C., Bode, R., Johnson, N., Quinn, C., Martens, W., McDermott, M.P., Rothrock, N., Thornton, C., Vickrey, B., Victorson, D. *et al.* (2012) Patient-reported impact of symptoms in myotonic dystrophy type 1 (PRISM-1). *Neurology*, **79**, 348–357.
12. Grimby, G., Hedberg, M., Henriksson, K.G., Johansson, G., Wigerstad-Lossing, I., Sellden, U. and Orndahl, G. (1988) Muscle function and morphology in myotonic dystrophy. *Acta Med. Scand.*, **224**, 349–356.
13. Bentzinger, C.F., Wang, Y.X., Dumont, N.A. and Rudnicki, M.A. (2013) Cellular dynamics in the muscle satellite cell niche. *EMBO Rep.*, **14**, 1062–1072.
14. Seale, P., Sabourin, L.A., Girgis-Gabardo, A., Mansouri, A., Gruss, P. and Rudnicki, M.A. (2000) Pax7 is required for the specification of myogenic satellite cells. *Cell*, **102**, 777–786.
15. Verdijk, L.B., Snijders, T., Drost, M., Delhaas, T., Kadi, F. and van Loon, L.J. (2014) Satellite cells in human skeletal muscle; from birth to old age. *Age (Dordr.)*, **36**, 545–547.
16. Yin, H., Price, F. and Rudnicki, M.A. (2013) Satellite cells and the muscle stem cell niche. *Physiol. Rev.*, **93**, 23–67.
17. Collins-Hooper, H., Woolley, T.E., Dyson, L., Patel, A., Potter, P., Baker, R.E., Gaffney, E.A., Maini, P.K., Dash, P.R. and Patel, K. (2012) Age-related changes in speed and mechanism of adult skeletal muscle stem cell migration. *Stem Cells*, **30**, 1182–1195.
18. Morgan, J.E. and Zammit, P.S. (2010) Direct effects of the pathogenic mutation on satellite cell function in muscular dystrophy. *Exp. Cell Res.*, **316**, 3100–3108.
19. Oexle, K. and Kohlschutter, A. (2001) Cause of progression in Duchenne muscular dystrophy: impaired differentiation

more probable than replicative aging. *Neuropediatrics*, **32**, 123–129.
20. Onofre-Oliveira, P.C., Santos, A.L., Martins, P.M., Ayub-Guerrieri, D. and Vainzof, M. (2012) Differential expression of genes involved in the degeneration and regeneration pathways in mouse models for muscular dystrophies. *NeuroMolecular Med.*, **14**, 74–83.
21. Pallafacchina, G., Blaauw, B. and Schiaffino, S. (2013) Role of satellite cells in muscle growth and maintenance of muscle mass. *Nutr. Metab. Cardiovasc. Dis.*, **23**, S12–S18.
22. Kudryashova, E., Kramerova, I. and Spencer, M.J. (2012) Satellite cell senescence underlies myopathy in a mouse model of limb-girdle muscular dystrophy 2H. *J. Clin. Invest.*, **122**, 1764–1776.
23. Amack, J.D., Paguio, A.P. and Mahadevan, M.S. (1999) Cis and trans effects of the myotonic dystrophy (DM) mutation in a cell culture model. *Hum. Mol. Genet.*, **8**, 1975–1984.
24. Amack, J.D. and Mahadevan, M.S. (2001) The myotonic dystrophy expanded CUG repeat tract is necessary but not sufficient to disrupt C2C12 myoblast differentiation. *Hum. Mol. Genet.*, **10**, 1879–1887.
25. Amack, J.D. and Mahadevan, M.S. (2004) Myogenic defects in myotonic dystrophy. *Dev. Biol.*, **265**, 294–301.
26. Amack, J.D., Reagan, S.R. and Mahadevan, M.S. (2002) Mutant DMPK 3'-UTR transcripts disrupt C2C12 myogenic differentiation by compromising MyoD. *J. Cell Biol.*, **159**, 419–429.
27. Gladman, J.T., Yadava, R.S., Mandal, M., Yu, Q., Kim, Y.K. and Mahadevan, M.S. (2015) NKX2-5, a modifier of skeletal muscle pathology due to RNA toxicity. *Hum. Mol. Genet.*, **24**, 251–264.
28. Furling, D., Coiffier, L., Mouly, V., Barbet, J.P., St Guily, J.L., Taneja, K., Gourdon, G., Junien, C. and Butler-Browne, G.S. (2001) Defective satellite cells in congenital myotonic dystrophy. *Hum. Mol. Genet.*, **10**, 2079–2087.
29. Furling, D., Lemieux, D., Taneja, K. and Puymirat, J. (2001) Decreased levels of myotonic dystrophy protein kinase (DMPK) and delayed differentiation in human myotonic dystrophy myoblasts. *Neuromuscul. Disord.*, **11**, 728–735.
30. Thornell, L.E., Lindstom, M., Renault, V., Klein, A., Mouly, V., Ansved, T., Butler-Browne, G. and Furling, D. (2009) Satellite cell dysfunction contributes to the progressive muscle atrophy in myotonic dystrophy type 1. *Neuropathol. Appl. Neurobiol.*, **35**, 603–613.
31. Loro, E., Rinaldi, F., Malena, A., Masiero, E., Novelli, G., Angelini, C., Romeo, V., Sandri, M., Botta, A. and Vergani, L. (2010) Normal myogenesis and increased apoptosis in myotonic dystrophy type-1 muscle cells. *Cell Death Differ.*, **17**, 1315–1324.
32. Song, K.Y., Guo, X.M., Wang, H.Q., Zhang, L., Huang, S.Y., Huo, Y.C., Zhang, G., Feng, J.Z., Zhang, R.R., Ma, Y. *et al.* (2020) MBNL1 reverses the proliferation defect of skeletal muscle satellite cells in myotonic dystrophy type 1 by inhibiting autophagy via the mTOR pathway. *Cell Death Dis.*, **11**, 545.
33. Kim, E.Y., Barefield, D.Y., Vo, A.H., Gacita, A.M., Schuster, E.J., Wyatt, E.J., Davis, J.L., Dong, B., Sun, C., Page, P. *et al.* (2019) Distinct pathological signatures in human cellular models of myotonic dystrophy subtypes. *JCI Insight*, **4**, e122686. https://doi.org/10.1172/jci.insight.122686.
34. Wang, Y., Hao, L., Wang, H., Santostefano, K., Thapa, A., Cleary, J., Li, H., Guo, X., Terada, N., Ashizawa, T. *et al.* (2018) Therapeutic genome editing for myotonic dystrophy type 1 using CRISPR/Cas9. *Mol. Ther.*, **26**, 2617–2630.
35. Mondragon-Gonzalez, R. and Perlingeiro, R.C.R. (2018) Recapitulating muscle disease phenotypes with myotonic dystrophy 1 induced pluripotent stem cells: a tool for disease modeling and drug discovery. *Dis. Model. Mech.*, **11**. doi: 10.1242/dmm.034728.
36. Ueki, J., Nakamori, M., Nakamura, M., Nishikawa, M., Yoshida, Y., Tanaka, A., Morizane, A., Kamon, M., Araki, T., Takahashi, M.P. *et al.* (2017) Myotonic dystrophy type 1 patient-derived iPSCs for the investigation of CTG repeat instability. *Sci. Rep.*, **7**, 42522.
37. Brun, C.E., Wang, Y.X. and Rudnicki, M.A. (2018) Single EDL myofiber isolation for analyses of quiescent and activated muscle stem cells. *Methods Mol. Biol.*, **1686**, 149–159.
38. Hardy, D., Besnard, A., Latil, M., Jouvion, G., Briand, D., Thepenier, C., Pascal, Q., Guguin, A., Gayraud-Morel, B., Cavaillon, J.M. *et al.* (2016) Comparative study of injury models for studying muscle regeneration in mice. *PLoS One*, **11**, e0147198.
39. Laurent, A., Pinset, C., Aurade, F., Vidaud, M. and Montarras, D. (1997) Expression of myotonic dystrophy protein kinase gene during in vivo and in vitro mouse myogenesis. *Cell. Mol. Biol. (Noisy-le-Grand)*, **43**, 881–888.
40. Paul, S., Dansithong, W., Kim, D., Rossi, J., Webster, N.J., Comai, L. and Reddy, S. (2006) Interaction of muscleblind, CUG-BP1 and hnRNP H proteins in DM1-associated aberrant IR splicing. *EMBO J.*, **25**, 4271–4283.
41. Holt, I., Jacquemin, V., Fardaei, M., Sewry, C.A., Butler-Browne, G.S., Furling, D., Brook, J.D. and Morris, G.E. (2009) Muscleblind-like proteins: similarities and differences in normal and myotonic dystrophy muscle. *Am. J. Pathol.*, **174**, 216–227.
42. Lin, X., Miller, J.W., Mankodi, A., Kanadia, R.N., Yuan, Y., Moxley, R.T., Swanson, M.S. and Thornton, C.A. (2006) Failure of MBNL1-dependent post-natal splicing transitions in myotonic dystrophy. *Hum. Mol. Genet.*, **15**, 2087–2097.
43. Mahadevan, M.S., Yadava, R.S., Yu, Q., Balijepalli, S., Frenzel-McCardell, C.D., Bourne, T.D. and Phillips, L.H. (2006) Reversible model of RNA toxicity and cardiac conduction defects in myotonic dystrophy. *Nat. Genet.*, **38**, 1066–1070.
44. Yadava, R.S., Yu, Q., Mandal, M., Rigo, F., Bennett, C.F. and Mahadevan, M.S. (2020) Systemic therapy in an RNA toxicity mouse model with an antisense oligonucleotide therapy targeting a non-CUG sequence within the DMPK 3'UTR RNA. *Hum. Mol. Genet.*, **29**, 1440–1453.
45. Yadava, R.S., Kim, Y.K., Mandal, M., Mahadevan, K., Gladman, J.T., Yu, Q. and Mahadevan, M.S. (2019) MBNL1 overexpression is not sufficient to rescue the phenotypes in a mouse model of RNA toxicity. *Hum. Mol. Genet.*, **28**, 2330–2338.
46. Yablonka-Reuveni, Z. (2011) The skeletal muscle satellite cell: still young and fascinating at 50. *J. Histochem. Cytochem.*, **59**, 1041–1059.
47. Charge, S.B. and Rudnicki, M.A. (2004) Cellular and molecular regulation of muscle regeneration. *Physiol. Rev.*, **84**, 209–238.
48. Cooper, R.N., Tajbakhsh, S., Mouly, V., Cossu, G., Buckingham, M. and Butler-Browne, G.S. (1999) In vivo satellite cell activation via Myf5 and MyoD in regenerating mouse skeletal muscle. *J. Cell Sci.*, **112**, 2895–2901.
49. Wang, Y.X. and Rudnicki, M.A. (2011) Satellite cells, the engines of muscle repair. *Nat. Rev. Mol. Cell Biol.*, **13**, 127–133.
50. von Maltzahn, J., Jones, A.E., Parks, R.J. and Rudnicki, M.A. (2013) Pax7 is critical for the normal function of satellite cells in adult skeletal muscle. *Proc. Natl. Acad. Sci. U. S. A.*, **110**, 16474–16479.

51. Greenberg, A.S., Egan, J.J., Wek, S.A., Moos, M.C., Jr., Londos, C. and Kimmel, A.R. (1993) Isolation of cDNAs for perilipins A and B: sequence and expression of lipid droplet-associated proteins of adipocytes. *Proc. Natl. Acad. Sci. U. S. A.*, **90**, 12035–12039.
52. Ostergaard, M.E., Jackson, M., Low, A., A, E.C., R, G.L., Peralta, R.Q., Yu, J., Kinberger, G.A., Dan, A., Carty, R. *et al.* (2019) Conjugation of hydrophobic moieties enhances potency of antisense oligonucleotides in the muscle of rodents and non-human primates. *Nucleic Acids Res.*, **47**, 6045–6058.
53. Prakash, T.P., Mullick, A.E., Lee, R.G., Yu, J., Yeh, S.T., Low, A., Chappell, A.E., Ostergaard, M.E., Murray, S., Gaus, H.J. *et al.* (2019) Fatty acid conjugation enhances potency of antisense oligonucleotides in muscle. *Nucleic Acids Res.*, **47**, 6029–6044.
54. Mankodi, A., Logigian, E., Callahan, L., McClain, C., White, R., Henderson, D., Krym, M. and Thornton, C.A. (2000) Myotonic dystrophy in transgenic mice expressing an expanded CUG repeat. *Science*, **289**, 1769–1773.
55. Huguet, A., Medja, F., Nicole, A., Vignaud, A., Guiraud-Dogan, C., Ferry, A., Decostre, V., Hogrel, J.Y., Metzger, F., Hoeflich, A. *et al.* (2012) Molecular, physiological, and motor performance defects in DMSXL mice carrying >1,000 CTG repeats from the human DM1 locus. *PLoS Genet.*, **8**, e1003043.
56. Lepper, C., Partridge, T.A. and Fan, C.M. (2011) An absolute requirement for Pax7-positive satellite cells in acute injury-induced skeletal muscle regeneration. *Development*, **138**, 3639–3646.
57. Murphy, M.M., Lawson, J.A., Mathew, S.J., Hutcheson, D.A. and Kardon, G. (2011) Satellite cells, connective tissue fibroblasts and their interactions are crucial for muscle regeneration. *Development*, **138**, 3625–3637.
58. Sambasivan, R., Yao, R., Kissenpfennig, A., Van Wittenberghe, L., Paldi, A., Gayraud-Morel, B., Guenou, H., Malissen, B., Tajbakhsh, S. and Galy, A. (2011) Pax7-expressing satellite cells are indispensable for adult skeletal muscle regeneration. *Development*, **138**, 3647–3656.
59. Storbeck, C.J., Sabourin, L.A., Waring, J.D. and Korneluk, R.G. (1998) Definition of regulatory sequence elements in the promoter region and the first intron of the myotonic dystrophy protein kinase gene. *J. Biol. Chem.*, **273**, 9139–9147.
60. Relaix, F. and Zammit, P.S. (2012) Satellite cells are essential for skeletal muscle regeneration: the cell on the edge returns Centre stage. *Development*, **139**, 2845–2856.
61. McCarthy, J.J., Mula, J., Miyazaki, M., Erfani, R., Garrison, K., Farooqui, A.B., Srikuea, R., Lawson, B.A., Grimes, B., Keller, C. *et al.* (2011) Effective fiber hypertrophy in satellite cell-depleted skeletal muscle. *Development*, **138**, 3657–3666.
62. Robson, L.G., Di Foggia, V., Radunovic, A., Bird, K., Zhang, X. and Marino, S. (2011) Bmi1 is expressed in postnatal myogenic satellite cells, controls their maintenance and plays an essential role in repeated muscle regeneration. *PLoS One*, **6**, e27116.
63. Solbakken, G., Bjornara, B., Kirkhus, E., Nguyen, B., Hansen, G., Frich, J.C. and Orstavik, K. (2019) MRI of trunk muscles and motor and respiratory function in patients with myotonic dystrophy type 1. *BMC Neurol.*, **19**, 135.
64. Cote, C., Hiba, B., Hebert, L.J., Vial, C., Remec, J.F., Janier, M. and Puymirat, J. (2011) MRI of tibialis anterior skeletal muscle in myotonic dystrophy type 1. *Can. J. Neurol. Sci.*, **38**, 112–118.
65. Hiba, B., Richard, N., Hebert, L.J., Cote, C., Nejjari, M., Vial, C., Bouhour, F., Puymirat, J. and Janier, M. (2012) Quantitative assessment of skeletal muscle degeneration in patients with myotonic dystrophy type 1 using MRI. *J. Magn. Reson. Imaging*, **35**, 678–685.
66. Peric, S., Maksimovic, R., Banko, B., Durdic, M., Bjelica, B., Bozovic, I., Balcik, Y., Pesovic, J., Savic-Pavicevic, D. and Rakocevic-Stojanovic, V. (2017) Magnetic resonance imaging of leg muscles in patients with myotonic dystrophies. *J. Neurol.*, **264**, 1899–1908.
67. Song, J., Fu, J., Ma, M., Pang, M., Li, G., Gao, L. and Zhang, J. (2020) Lower limb muscle magnetic resonance imaging in Chinese patients with myotonic dystrophy type 1. *Neurol. Res.*, **42**, 170–177.
68. Fry, C.S., Kirby, T.J., Kosmac, K., McCarthy, J.J. and Peterson, C.A. (2017) Myogenic progenitor cells control extracellular matrix production by fibroblasts during skeletal muscle hypertrophy. *Cell Stem Cell*, **20**, 56–69.
69. Fry, C.S., Lee, J.D., Jackson, J.R., Kirby, T.J., Stasko, S.A., Liu, H., Dupont-Versteegden, E.E., McCarthy, J.J. and Peterson, C.A. (2014) Regulation of the muscle fiber microenvironment by activated satellite cells during hypertrophy. *FASEB J.*, **28**, 1654–1665.
70. Fry, C.S., Lee, J.D., Mula, J., Kirby, T.J., Jackson, J.R., Liu, F., Yang, L., Mendias, C.L., Dupont-Versteegden, E.E., McCarthy, J.J. *et al.* (2015) Inducible depletion of satellite cells in adult, sedentary mice impairs muscle regenerative capacity without affecting sarcopenia. *Nat. Med.*, **21**, 76–80.
71. Jackson, J.R., Kirby, T.J., Fry, C.S., Cooper, R.L., McCarthy, J.J., Peterson, C.A. and Dupont-Versteegden, E.E. (2015) Reduced voluntary running performance is associated with impaired coordination as a result of muscle satellite cell depletion in adult mice. *Skelet. Muscle*, **5**, 41.
72. Kinney, M.C., Dayanidhi, S., Dykstra, P.B., McCarthy, J.J., Peterson, C.A. and Lieber, R.L. (2017) Reduced skeletal muscle satellite cell number alters muscle morphology after chronic stretch but allows limited serial sarcomere addition. *Muscle Nerve*, **55**, 384–392.
73. Englund, D.A., Murach, K.A., Dungan, C.M., Figueiredo, V.C., Vechetti, I.J., Jr., Dupont-Versteegden, E.E., McCarthy, J.J. and Peterson, C.A. (2020) Depletion of resident muscle stem cells negatively impacts running volume, physical function, and muscle fiber hypertrophy in response to lifelong physical activity. *Am. J. Physiol. Cell Physiol.*, **318**, C1178–C1188.
74. Olguin, H.C. and Pisconti, A. (2012) Marking the tempo for myogenesis: Pax7 and the regulation of muscle stem cell fate decisions. *J. Cell. Mol. Med.*, **16**, 1013–1025.
75. Olguin, H.C., Yang, Z., Tapscott, S.J. and Olwin, B.B. (2007) Reciprocal inhibition between Pax7 and muscle regulatory factors modulates myogenic cell fate determination. *J. Cell Biol.*, **177**, 769–779.
76. Wosczyna, M.N. and Rando, T.A. (2018) A muscle stem cell support group: coordinated cellular responses in muscle regeneration. *Dev. Cell*, **46**, 135–143.
77. Wosczyna, M.N., Konishi, C.T., Perez Carbajal, E.E., Wang, T.T., Walsh, R.A., Gan, Q., Wagner, M.W. and Rando, T.A. (2019) Mesenchymal stromal cells are required for regeneration and homeostatic maintenance of skeletal muscle. *Cell Rep.*, **27**, 2029–2035 e2025.
78. Santini, M.P., Malide, D., Hoffman, G., Pandey, G., D'Escamard, V., Nomura-Kitabayashi, A., Rovira, I., Kataoka, H., Ochando, J., Harvey, R.P. *et al.* (2020) Tissue-resident PDGFRalpha(+) progenitor cells contribute to fibrosis versus healing in a context- and spatiotemporally dependent manner. *Cell Rep.*, **30**, 555–570 e557.
79. Biferali, B., Proietti, D., Mozzetta, C. and Madaro, L. (2019) Fibro-adipogenic progenitors cross-talk in skeletal muscle: the social network. *Front. Physiol.*, **10**, 1074.

80. Farup, J., Madaro, L., Puri, P.L. and Mikkelsen, U.R. (2015) Interactions between muscle stem cells, mesenchymal-derived cells and immune cells in muscle homeostasis, regeneration and disease. *Cell Death Dis.*, **6**, e1830.
81. Joe, A.W., Yi, L., Natarajan, A., Le Grand, F., So, L., Wang, J., Rudnicki, M.A. and Rossi, F.M. (2010) Muscle injury activates resident fibro/adipogenic progenitors that facilitate myogenesis. *Nat. Cell Biol.*, **12**, 153–163.
82. Uezumi, A., Ito, T., Morikawa, D., Shimizu, N., Yoneda, T., Segawa, M., Yamaguchi, M., Ogawa, R., Matev, M.M., Miyagoe-Suzuki, Y. *et al.* (2011) Fibrosis and adipogenesis originate from a common mesenchymal progenitor in skeletal muscle. *J. Cell Sci.*, **124**, 3654–3664.
83. Mazala, D.A., Novak, J.S., Hogarth, M.W., Nearing, M., Adusumalli, P., Tully, C.B., Habib, N.F., Gordish-Dressman, H., Chen, Y.W., Jaiswal, J.K. *et al.* (2020) TGF-beta-driven muscle degeneration and failed regeneration underlie disease onset in a DMD mouse model. *JCI Insight*, **5**, e135703. https://doi.org/10.1172/jci.insight.135703.
84. Hogarth, M.W., Defour, A., Lazarski, C., Gallardo, E., Diaz Manera, J., Partridge, T.A., Nagaraju, K. and Jaiswal, J.K. (2019) Fibroadipogenic progenitors are responsible for muscle loss in limb girdle muscular dystrophy 2B. *Nat. Commun.*, **10**, 2430.
85. Rehman, S., Gladman, J.T., Periasamy, A., Sun, Y. and Mahadevan, M.S. (2014) Development of an AP-FRET based analysis for characterizing RNA-protein interactions in myotonic dystrophy (DM1). *PLoS One*, **9**, e95957.
86. Langlois, M.A., Lee, N.S., Rossi, J.J. and Puymirat, J. (2003) Hammerhead ribozyme-mediated destruction of nuclear foci in myotonic dystrophy myoblasts. *Mol. Ther.*, **7**, 670–680.